REVIEW

Check for updates

Metallic nanosponges for energy storage and conversion applications

N. R. Hemanth, †[a] Ranjit D. Mohili, †[b] Monika Patel, [b] Arvind H. Jadhav, [c] Kwangyeol Lee *[d] and Nitin K. Chaudhari *[b]

In order to meet the current energy storage demands, the rational design of novel nanostructured materials is crucial for the improvement of electrochemical storage and conversion performance. Nanostructured materials have shown promising results in various energy harvesting systems, owing to their multifunctional properties such as a large active surface area, mechanical strength, catalytic ability, excellent ion diffusion, and electronic conductivity. To date, the library of nanostructured materials consists of diverse compositions ranging from oxides, dichalcogenides, carbides to graphene-based and lithium alloys with various morphologies such as zero-dimensional (0D), 1D, 2D and 3D nanomaterials. In particular, nanosponges have exhibited unusual three-dimensional architecture that provides rich surface defects and excellent structural stability resulting in improved catalytic activity. Additionally, the large conducting surface, electronic conductivity and pronounced crystalline phase stability of nanosponges have been utilized to improve the electrode performance drastically. Moreover, the unique sponge-like metallic porous network not only reduces the overall weight of the device but also decreases the consumption of metal usage. In this context, this review particularly highlights the recent progress in the synthesis and properties of noble metals and other metal-based sulphide, oxide, hydroxide and phosphide nanosponges, and their application in electrochemical storage and conversion devices.

[a]*Department of Metallurgical and Materials Engineering, National Institute of Technology Karnataka (NITK), Surathkal, Karnataka, India*

[b]*Department of Chemistry, School of Technology, Pandit Deendayal Energy University, Gandhinagar 382007, Gujarat, India. E-mail: nitin.chaudhari@sot.pdpu.ac.in*

[c]*Centre for Nano and Material Science (CNMS), Jain University, Jain Global Campus, Bangalore 562112, Karnataka, India*

[d]*Department of Chemistry, Research Institute for Natural Sciences, Korea University, Seoul 02841, Republic of Korea. E-mail: kylee1@korea.ac.kr*

† These authors contributed equally to this work.

Professor Kwangyeol Lee obtained his Ph.D. degree (1997) in Chemistry from the University of Illinois at Urbana-Champaign. After fulfilling his military obligation, he joined Korea University in 2003 as a chemistry faculty member, before being appointed as a professor. His current interests include the development of synthetic methodologies for nanoscale materials and the development of nanotechnologies to support sustainable energy sources.

Dr Nitin Chaudhari is an Associate Professor at Pandit Deendayal Energy University, Gandhinagar, India. He received his Ph.D. degree in Materials Science from Korea University, South Korea in 2013. He subsequently worked as a Research Professor at Myongji University and Korea University, South Korea from 2013 to 2019. Later, he joined Nexcoms Ltd Co., South Korea as a Deputy Director before moving to India. His research interests include the design and development of active electrode materials such as porous carbons, nanocomposites, oxides, sulphides, hydroxides, 2D MXenes, and nanomaterials for energy storage and conversion devices.

This journal is © The Royal Society of Chemistry 2022

J. Mater. Chem. A, 2022, **10**, 14221–14246 | **14221**

1. Introduction

Enhanced accessibility to energy supply, driven by economic growth, has accelerated the present industrial and consumer demands to newer heights. Due to the finite supply of fossil fuel and global impact of carbon emission, the electrical energy generated from renewable resources has received considerable attention.[1,2] However, renewable resources such as solar and wind energy are intermittent, and thus the design of robust electrical energy storage and conversion systems is very crucial.[3] Various electrochemical storage and conversion technologies, such as batteries, supercapacitors, fuel cells, and electrolysers, have been developed in recent decades.[4–7] Although considerable growth has been seen in recent years for these technologies, still great challenges exist for their commercial applications in electric vehicles, portable electronics, and grid-scale energy storage. The potential to improve the performance and efficiency of these devices is largely dependent on the materials they are made of, which has prompted the emergence of advanced nanostructured materials.[8]

Nanostructured materials have sparked significant research interest in electrochemical energy devices over the last two decades due to their excellent properties, opening new possibilities for overcoming device limitations.[9–11] Their advantageous properties include electrical, chemical, and mechanical aspects, nanoscale confinement effects, and surface properties.[9,12] The family of nanostructured materials has a wide range of electrochemical properties and rich chemistry due to diverse compositions ranging from oxides, carbides, dichalcogenides to carbon-based, lithium alloys, and conducting polymers, among others.[13–18] Nanomaterials can exist in various morphologies such as zero-dimensional (0D) quantum dots and nanoparticles;[19,20] one-dimensional (1D) nanotubes, nanofibers, and nanowires;[13,21] two-dimensional (2D) nanolayers and nanoflakes;[22,23] three-dimensional (3D) porous networks.[24–26] However, despite the increasing number of nanostructured materials with intriguing features, none can solve all the current energy storage limitations at the same time. For example, 0D and 1D nanostructures have lower electrical conductivity and lower volumetric capacitance, respectively, but these limits can be circumvented by combining them together, resulting in higher volumetric capacitance.[27] The main obstacles for 2D nanostructures are restacking of layers and poor kinetics, which hybrid 2D structures can solve by providing a stable structure and rapid ion transportation.[28] On the other hand, 3D nanostructures are assemblies of 0D, 1D, and 2D nanostructures of the same kind and have excellent inherent features like a high specific surface area and increased active sites.[27,29] Optimized design and fabrication of these nanostructures is key to decreasing the overall weight and space of electrochemical devices and reducing material usage.[27] In particular, sponge-like nanostructures are low in density and provide collective features suitable for a wide range of electrochemical energy applications.[30,31]

Nanosponge materials have an unusual porous structure that resembles metallic foam or sponges as the majority of volume (about 75–95%) is void.[32,33] As a result, the low density nanosponge greatly enhances the electrode–electrolyte interaction compared to bulk high density nanostructures. This is mainly attributed to the large specific area and rapid mass transportation due to the creation of sponge-like structures. The general approach employed for the synthesis of nanosponges includes dealloying, hydrothermal, electrochemical deposition, kinetics-controlled reactions and template-based techniques.[34–38] These synthetic strategies have resulted in the formation of various compositions of nanosponges, which have demonstrated promising performances in catalysis and energy storage. In addition, the doping of nanosponge with different elements has further improved their electrochemical performances.[39,40] Therefore, the rational design of nanosponges can address the energy storage issues and economical usage of materials.

Till date, numerous reviews have been dedicated to the design, synthesis and characterization of nanostructured materials for energy storage and conversion applications,[8,9,12,27,30,41] and carbon-based nanostructured materials are ubiquitous.[16,42–45] However, to the best of our knowledge, there exists no critical review that specifically emphasizes nanosponge materials for electrochemical energy applications, despite their promising results as electrode and catalyst materials (Fig. 1). Therefore, we aim to provide an overview of recent advances in nanosponge materials, particularly based on noble metals and non-noble metal-based oxides, hydroxides, sulphides and phosphides (Fig. 2). From the synthesis perspective, this review highlights recent developments in synthetic methodologies and fabrication techniques. Furthermore, the electrochemical applications of nanosponges are outlined. Finally, the summary of the current research and challenges provides future prospects for developing lightweight and cost-effective energy storage and conversion systems.

2. Classification of metallic nanosponges

Porous nanostructures have been extensively studied for energy storage and conversion.[46,47] They are classified as microporous (2 nm), mesoporous (2–50 nm), and macroporous (>50 nm)
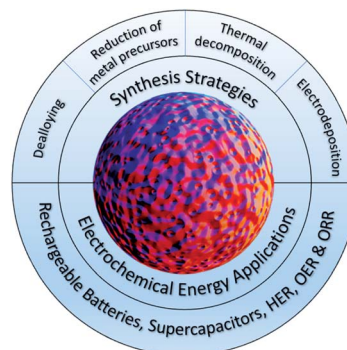

Fig. 1 Graphical abstract of nanosponges and their synthesis and electrochemical energy applications.

14222 | *J. Mater. Chem. A*, 2022, **10**, 14221–14246

This journal is © The Royal Society of Chemistry 2022

Fig. 2 Different types of metals (yellow), non-metals (blue), and dopants (green) explored in nanosponge synthesis.

based on their size as well as ordered and non-ordered porous materials based on their morphologies.[48] Among the non-ordered porous materials such as nanosponges, hollow structures, highly branched nanomaterials and aerogels, metallic nanosponge materials are of interest because of their unique combination of electrical, catalytic, and mechanical properties. The nanosponge structure creates an interlinked channel at the nanoscale which results in a large surface area and improved charge and mass transfer. In addition to their attractive electrochemical properties, they have also displayed magnetic, superior absorption, mechanical stability, and semiconductor properties that have opened a wide range of applications. The synthesis and properties of metallic nanosponge materials are discussed in detail in this section.

2.1 Monometallic nanosponges

Monometallic nanosponges refer to the primary type of nanosponge containing a single metal. A template-based approach is commonly utilized to synthesise metal and metal oxide-based nanosponges.[49–51] However, template-assisted methods have not produced desirable results with pristine noble metals because they require post-synthesis template removal processes.[52,53] Hence a template-free and sacrificial template approach that does not require an additional template removal process is currently developed. For example, by employing sucrose as the sacrificial soft template, a large scale synthesis of transition metal (Cu, Co and Ni) nanosponges with excellent catalytic properties has been accomplished by heating a mixture of sucrose and metal salts.[52] Furthermore, to reduce the multiple steps and make the process amenable to a large number of metals, a rapid one-step process *via* kinetically controlled borohydride reduction was developed to synthesise noble metal (Au, Ag, Pt, and Pd) nanosponges.[53] This method was further extended to the fabrication of Ru nanosponges, which have found applications in optoelectronic nanodevices. In a recent study, monometallic nanosponges have displayed superior catalytic activity compared to their bulk analogues.[54]

Specifically, amongst the Ag, Au, Pt, Pd and Cu nanosponges, palladium has displayed the highest hydrogen sorption and catalytic activity with a great structural retention after catalytic operation.[54] Although monometallic nanosponges have gained significant research interest in the application of catalysis,[52,54,55] optical sensors[53] and hydrogen storage,[54] bimetallic and polymetallic nanosponges seem to exhibit overall better performance due to the synergy of multiple metals.[56]

2.2 Bimetallic nanosponges

Bimetallic nanosponges display superior properties to their monometallic counterparts due to tuneable properties resulting from the synergistic effect of combining different components.[34] Dealloying is one of the preferred approaches for the synthesis of bimetallic nanosponges, and Yan *et al.* fabricated Ag–Au hybrid nanosponges, with excellent plasmonic properties, by solid state dewetting of Au/Ag layers followed by dealloying of Au nanosponges in nitric acid.[57] Further research on this process reveals that the dealloying time plays a crucial role in achieving high-yield formation of sponge-like Au–Ag nanocubes; the increase in time led to an increase in the pore size.[58] Au–Ag nanosponges have exhibited outstanding performance in electrochemical catalysis, plasmonic, surface-enhanced Raman spectroscopy, *etc.*, due to their highly porous structure with abundant active sites; the presence of Au stabilizes Ag from oxidation so that active sites could function for a longer period.[58,59] Pt-based bimetallic alloys have also been explored because of superior catalytic activities, reduced Pt loading, and increased resistance to Pt poisoning.[60] Since the addition of early transition metals has been proven to improve catalytic efficiency and reduce Pt-based nanosponges cost,[60,61] a general strategy has been developed for producing PtM (M = Fe, Co, Cu, Ni) bimetallic nanosponges in the presence of aluminium.[62] The addition of Al facilitated the formation of a 3D structure, and the resulting nanosponges displayed excellent catalytic performance. PtFe nanosponges, in particular, displayed excellent oxygen reduction reaction (ORR) performance. Zhu

This journal is © The Royal Society of Chemistry 2022

J. Mater. Chem. A, 2022, **10**, 14221–14246 | **14223**

et al. reported the synthesis of PdPt bimetallic nanosponges in the absence of a capping agent and further employed the same technique to produce Au and Pt based alloy nanosponges.[63] For direct alcohol fuel cells, the as-prepared PdPt nanosponges exhibited promising electrocatalytic properties. Because of the high cost and scarcity of Pt, Pd-based bimetallic alloy nanosponges are being studied extensively.[64] While Au, Ag, Pt and Pd based bimetallic nanosponges have been under a great research focus, other combinations of bimetallic alloy nanosponges such as Cu and Ni are also emerging.[36,56,65–67]

2.3 Multimetallic nanosponges

Multimetallic nanosponges are composed of more than two metallic constituents. The addition of a third metal component to bimetallic catalysts can significantly alter the surface strain effect and electronic properties, thus enhancing the overall performance of alloy catalysts. Lee *et al.* reported trimetallic Pd/Ag/Au nanosponges with a nanowire network by *in situ* self-regulated reduction of sodium dodecyl sulphate.[68] The second and third metals were added as precursor metal salts during synthesis, not requiring any reducing agent.[68] The diameter of the nanowires in the nanosponges was determined by the alloy nanomaterial used.[68] Li *et al.* suggested a surfactant-free approach to produce Pd-based multimetallic nanosponges with diverse combinations. Among the numerous compositions, $Pd_{62}Au_{21}Ni_{17}$ nanosponge showed excellent catalytic performance and stability in an alkaline medium, surpassing those of commercial Pt/C catalysts.[69] In recent years, hydrogen bubbles as a dynamic template have gained considerable research interest in electrochemical catalysis.[66] Shi *et al.* prepared $Pt_{53}Ru_{39}Ni_8$ nanosponges with a clean surface by a one-pot co-reduction wet chemical method using hydrogen bubbles as a dynamic template.[70] This trimetallic nanosponge exhibited a great electrocatalytic performance for hydrogen evolution and hydrazine oxidation reactions. Thus far, only trimetallic nanosponges have been reported, calling for further development to untap the great variety of compositions and excellent research opportunities.

3. Synthesis of nanosponges

The design of metallic nanosponges with a large surface area, rapid kinetics, and structural stability can significantly reduce materials usage and build cost-efficient energy devices. Thus far, metallic nanosponges have been prepared by dealloying, chemical reduction, electrodeposition, and thermal processes for diverse applications. Recent advances in these synthesis methods to develop noble and non-noble metallic nanosponges are discussed in the following subsections.

3.1 Dealloying

Dealloying is a versatile method to synthesize porous nanosponge materials. In this process, the less noble element is selectively etched from the alloy, leading to compositions primarily made up of more noble constituents.[71] The less noble metal can be etched in bulk or thin films, which can occur *via*

two routes, either by chemical dealloying or electrochemical dealloying.[72]

3.1.1 Chemical dealloying. In this process, highly corrosive acids (*e.g.*, nitric acid) are used for the removal of less noble constituents, leaving behind a sponge-like structure (Fig. 3a).[73] However, to trigger the etching process, the composition of the leaching element should be higher than the parting limit, which varies depending on the alloys. The preparation of nanoporous gold by selective leaching of silver from the Au–Ag alloy is a typical example of chemical dealloying.[74,75] Nanoporous gold (Fig. 3b and c) has been found to possess intriguing properties of high electrical conductivity, increased active sites, a large surface area, and enhanced mechanical stability.[76] Hence, the sponge-like porous structure arising due to dealloying in acidic medium has been extensively studied and has shown potential applications in several domains.[77–79] Zielasek *et al.* prepared sponge-like nanoporous Au by chemical dealloying of the Au–Ag alloy (70% of Ag) in nitric acid (HNO_3) and estimated the final Ag content to be less than 1% using atomic absorption spectroscopy.[75] Another study on Au-based nanosponges reported by Mel *et al.* described the selective dissolution of copper from Au–Cu thin films in HNO_3.[73] After a specific dealloying time, the films were washed in deionized water to stop further etching and remove residual acid. It was observed that the initial percentage of Au has an inverse relationship with the dissolution kinetics of Cu, which is due to the surface migration and coalescence of less coordinated Au atoms resulting in local passivation. Importantly, the study demonstrated the dealloying of non-homogeneous Au–Cu films and found that HNO_3 attacks the films laterally rather than perpendicularly (Fig. 4a–d). The co-leaching of two different metals from a ternary alloy to produce nanosponges has also been studied in recent years.
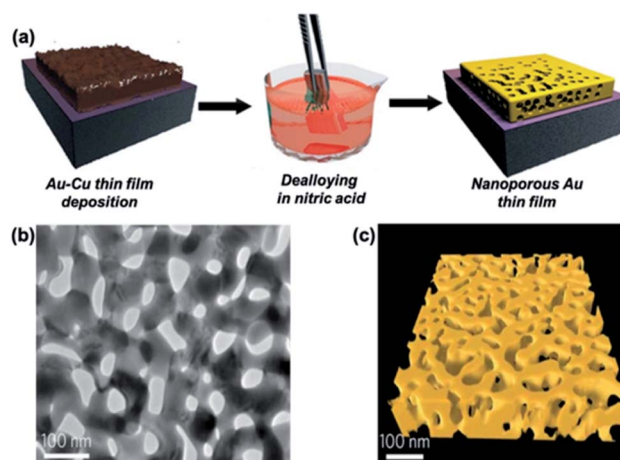

Fig. 3 Chemical dealloying of nanoporous gold. (a) Schematic representation of the chemical dealloying process to prepare nanoporous Au thin films by etching the Au−Cu alloy in nitric acid. Reproduced with permission.[73] Copyright 2015, American Chemical Society. (b) and (c) Bright-field TEM image and TEM tomography of nanoporous gold show nanopores of ∼30 nm size with a bicontinuous 3D structure. Reproduced with permission.[74] Copyright 2012, Springer Nature.

14224 | *J. Mater. Chem. A*, 2022, **10**, 14221–14246

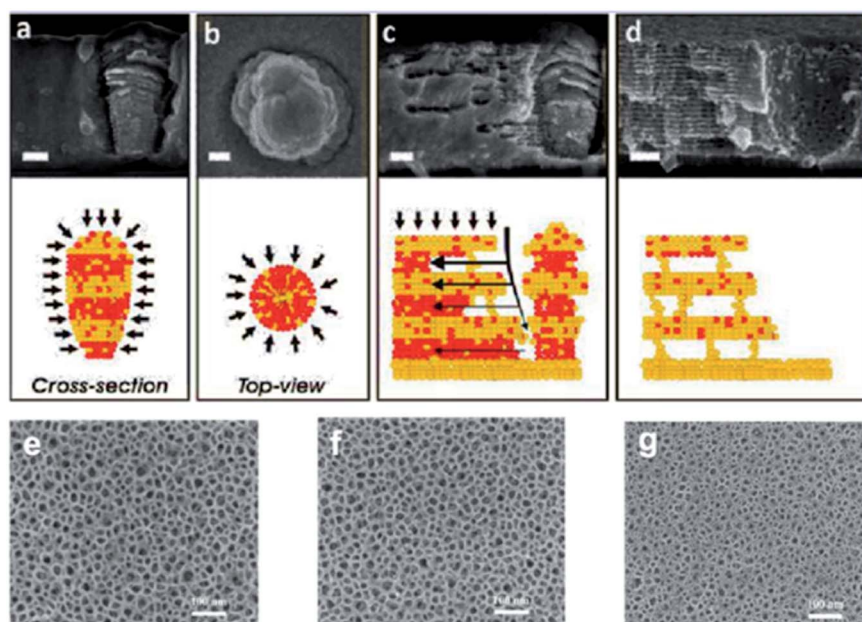This journal is © The Royal Society of Chemistry 2022

Fig. 4 Nanostructures after dealloying for different time periods and acids. SEM images (top) and schematic representation (bottom) of the lateral etching mechanism of Au–Cu films in HNO$_3$ for (a) and (b) 0.5 min, (c) 1 min, and (d) 5 min. Reproduced with permission.[73] Copyright 2015, American Chemical Society. SEM images of dealloyed S-NPMs in citric acid (e) at 1 g L^{-1} for 10 min, (f) at 0.5 g L^{-1} for 30 min, and (g) at 2 g L^{-1} for 60 min. Reproduced with permission.[81] Copyright 2016, Springer.

Li *et al.* showed that the incorporation of Ag into the Au–Cu binary alloy accelerated the leaching kinetics of Cu and also suppressed ligament coarsening.[80] The simultaneous leaching of Ag and Cu from the Au–Ag–Cu alloy in HNO$_3$ solution optimized the surface area to mass ratio and specific activities, and after complete dealloying the residual Ag stabilized the nanostructure and active sites. On the other hand, dealloying using citric acid can cause the formation of finer ligaments and can also act as a capping agent (Fig. 4e–g).[81] In this regard, Xu *et al.* employed citric acid to synthesize sponge-like nanoporous metals (Cu, Ni and Ag) by dealloying Mg$_{65}$M$_{25}$Y$_{10}$ (M = Cu, Ag, and Ni, at%) metallic glass ribbons as a precursor.[81] According to the report by Barman and Nanda, metallic (Ag, Cu and Sn) and bimetallic sponges (Cu–M, M = Ag, Au, Pt and Pd) were prepared by etching of a low reduction potential metal with sulfuric acid (H$_2$SO$_4$).[82] The application of H$_2$SO$_4$ led to a high yield synthesis without side product formation and prevented the oxide formation. The acid concentration and etching time can control the degree of etching and structural features; for a fixed time, increasing the concentration of HNO$_3$ for dealloying the Au–Cu alloy led to an increase in Cu leaching to give a bigger pore size and thicker ligaments.[83] While nitric acid is the most commonly used etchant for chemical dealloying due to strong oxidizing nature, other etchants such as citric acid, ferric nitrate, sulfuric acid, and ammonia have also been reported.[75,81–83] It is important to note that dealloying does not entirely remove the less noble metal and that the residual remaining of less noble metal can significantly improve the electrocatalytic activity.[80]

3.1.2 Electrochemical dealloying. Another dealloying approach is to apply anodic potential for selective dissolution of more reactive species from the alloy, in which the applied potential must be greater than the threshold potential of the dissolution species.[84] This is a thermodynamic measure that depends on the electrolyte, additives, and composition of the alloy. As discussed earlier, the synthesis of gold nanosponges by a dealloying process is an exemplary case; Cattarin *et al.* reported anodic leaching of Ag from the Ag$_{75}$Au$_{25}$ alloy in perchloric acid (HClO$_4$) at a potential of $E = 1.00$ V.[85] Electrochemical impedance spectroscopy characterization under dissolution conditions displayed capacitive behaviour with faradaic processes occurring at the lateral pore surface and pore bottom respectively. Electrochemical dealloying can also produce bulk nanoporous gold with retained defects and surface properties even after removing the majority of Ag from the parent alloy.[86] Sun and Balk mentioned a two-step galvanostatic dealloying method with different etching concentrations of HNO$_3$ in each stage and an external potential of $E = 1.00$ V to synthesize crack-free bulk nanoporous gold having a sponge-like structure with no volume change.[86] Mesoporous sponge-like materials prepared from a template-free method have been continuously developed in recent years because of their ordered mesoporosity and large surface area.[87] A report by Tominaka *et al.* described the preparation of a mesoporous PdCo sponge-like structure by dealloying electrodeposited PdCo thin films in nitrogen saturated H$_2$SO$_4$ solution at 0.6 V potential.[88] Very recently, Chen *et al.* reported a unique method to fabricate Pd nanosponges by dealloying a Ti$_{40}$Zr$_{10}$Cu$_{36}$Pd$_{14}$ amorphous alloy in a mixture of ammonium fluoride and ammonium sulphate solution at a current density of 10 mA cm^{-2}.[89] The structural and chemical uniformity with the crystallographic defect-free features of amorphous precursors can

promote the formation of fine and consistent pores; hence amorphous precursors were selected instead of a crystalline alloy. Electrochemical dealloying provides precise control over the dealloying of less noble metals from the alloy. However, chemical dealloying is more preferred owing to the easy operation.[73]

3.2 Reduction of metal precursors

The synthesis of nanostructured materials by reducing metal precursors is a powerful strategy as it offers precise control over the structural properties. Metallic nanosponges can be prepared via template supported or template-free reduction of metal precursors by using reducing agents. Thus, the prepared nanosponges have shown impressive performances in electrochemical energy applications.

3.2.1 Template-based formation of metal sponges. Template-based synthesis is the most convenient replication method for a diverse range of nanostructured materials with regulated nanoscale features. Nanostructured materials of desired morphologies, such as nanoparticles, nanopores, nanosheets, nanoflakes, nanotubes, etc., can be produced on a large scale, by using a template with well-defined structures (Fig. 5). A simple template-based synthesis process would involve three basic steps: (1) design and preparation of the original template with a definite porous structure, (2) filling of the template pores with the target material and then solidifying by an appropriate method, (3) removal of the original template leaving behind a metallic porous nanostructure. Until now, various hard and soft templates have been studied for the synthesis of metallic sponge-like structures.
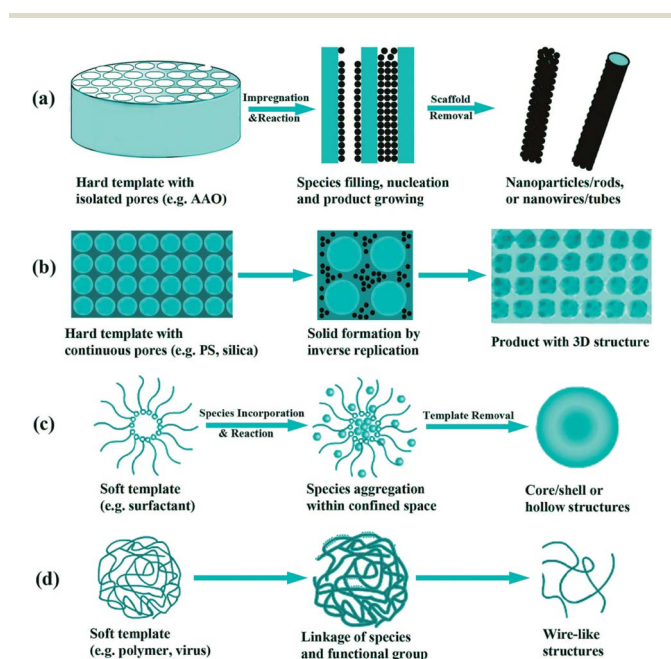

Fig. 5 Schematic representation of template-based synthesis of nanostructures. (a) and (b) Examples for hard templates and (c) and (d) examples for soft templates. Reprinted with permission.[90] Copyright 2008, American Chemical Society.

Hard templates. Hard templates (Fig. 5a and b) have a solid structure and a well-confined void, and their structural integrity is undisturbed by metal precursor infiltration.[90] Porous solids, colloidal crystals, aluminium oxide membranes, zeolites, and silica are among the hard templates employed to synthesize ordered meso/macro-structures.[48,72] The process involves impregnating precursors into a hard template, and then reducing either by a chemical or an electrochemical means, followed by heating at high temperature to connect metal nanoparticles within the template and removal of the template.[48] The connectivity of channels, surface characteristics and pore size of the template directly influence the properties of the end product. Cheng et al. discussed the different kinds of final structures formed, based on the pore connectivity of hard templates.[90] Templates having continuous pore channels (e.g. silica gels and porous carbon) yield a facsimile of templates with an interconnected porous network, whereas non-continuous templates (e.g. aluminium oxide membranes and MCM-41 silica) yield a replica of void space of template resembling nanotube-like structures.[90] The replication technique using mesoporous silicate templates is an efficient way to prepare 3D nanostructured materials such as Pd, Pt and Os with good catalytic activity.[91,92] To obtain high yield uniform sized particles, Wang et al. proposed the synthesis of mesoporous Pt nanoparticles by using silica templates (KIT-6 and SBA-15) and chemically reducing with ascorbic acid (AA).[93] When sodium borohydride and dimethylaminoborane were used instead of AA, an irregular and disordered porous structure was observed, implying that reducing agent strength is critical for obtaining a uniform porous structure. Nanoporous Pt sponges using silica templates (e.g. MCM-41, 48 and SBA-15) (Fig. 6a and b) were reported by Shin and co-workers, wherein the impregnated Pt precursor tetraammineplatinum(II) nitrate was reduced under a H_2 atmosphere at high temperature and subsequently washed with HF to remove the silica template.[94] A large number of continuous and discrete porous metals prepared using aluminium nanoparticle templates have been reported by Clay et al.[95] Chang et al. used a sponge-like 3D NiOOH/Ni(OH)$_2$ film with desired attributes as a hard template to fabricate nanostructured materials of different sizes and morphologies.[96]

Soft templates. Soft template synthesis offers various advantages compared to hard templates, including relatively benign conditions and ease of experimental operation. Soft templates are often structure-directing agents composed of amphiphilic molecules such as surfactants and amphiphilic block copolymers (Fig. 5c and d). When mixed in water, the surfactant molecules can self-assemble as spherical micelles above the critical micelle concentration. Increasing the surfactant concentration induces a lyotropic liquid crystal (LLC) phase, with long-range periodicity and lattice parameters of about 2–15 nm. LLC nanostructures can function as soft templates for the growth of porous metal structures on the surfactant.[97] Furthermore, soft templates can be eliminated carefully by chemical or thermal treatment at low temperatures. The evolvement of porous platinum structures by chemical reduction[98] or electrodeposition[99] of platinum salts within the

14226 | J. Mater. Chem. A, 2022, 10, 14221–14246

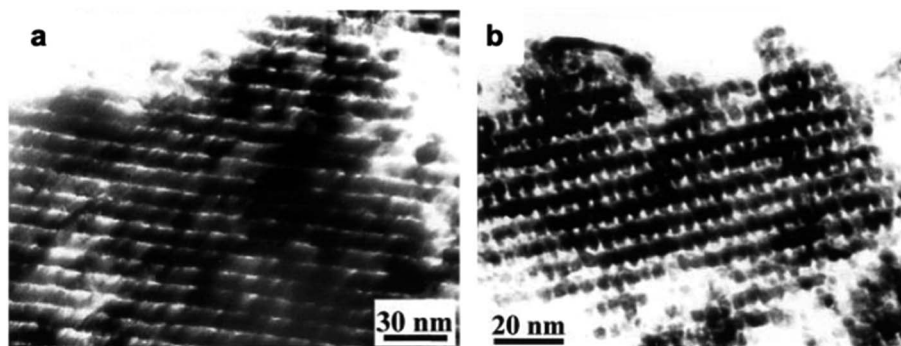This journal is © The Royal Society of Chemistry 2022

Fig. 6 TEM images of nanoporous platinum sponges revealing an interconnected and ordered structure. (a) Fabricated with SBA-15. (b) Fabricated with MCM-48. Reprinted with permission.[94] Copyright 2001, Royal Society of Chemistry.

aqueous domains of LLC phases has paved a way for new mesoporous noble metal fabrication.[100,101] However, the practice of the LLC synthesis approach is challenging,[102] because the homogeneous introduction of LLC into restrained quarters is difficult due to its high viscosity, restricting only to the fabrication of particle and thin-films.[103] Hence, Yamauchi and co-workers outlined an evaporation-mediated direct template (EDIT) process (Fig. 7a) that produced LLC phases consistently in low viscosity and dilute surfactant solutions.[103] They reported sponge-like Pt nanostructures obtained by displacement plating

between foam and a Pt complex after the LLC phase was created within Ni foam by solution evaporation (Fig. 7b).[104] The interface assisted synthesis method offers a non-equilibrium environment and high surface energy for the nucleation of nanostructures with desired morphologies.[105] Dong et al. reported the formation of spongy-like MnO_2 by a redox reaction of $KMnO_4$ and $NaBH_4$ in a bi-phase solution of toluene/H_2O, guided by tetraoctylammonium bromide (TOAB) as a soft template.[50] The presence of TOAB favoured the self-assembly of sponge-like MnO_2 nanoparticles at the interface by van der
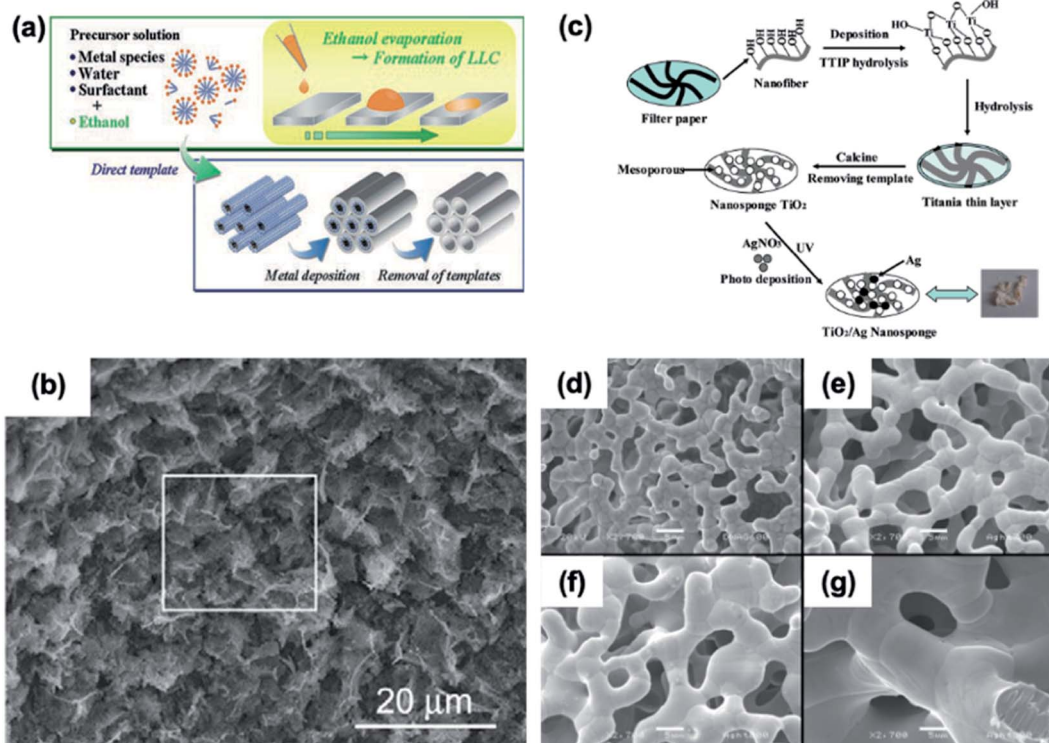
Fig. 7 Soft template approach for preparing nanosponge structures. (a) Schematic representation of the EDIT synthesis process. Reprinted with permission.[103] Copyright 2008, Wiley-VCH. (b) FE-SEM image of the Ni surface after Pt deposition. Reprinted with permission.[104] Copyright 2007, Elsevier. (c) Schematic representation of the TiO_2/Ag nanosponge synthesis process using natural cellulose as the soft template. Reprinted with permission.[107] Copyright 2012, American Chemical Society. SEM images of a silver nanosponge prepared at different temperatures: (d) 600 °C, (e) 700 °C, (f) 800 °C and (g) 900 °C. Reprinted with permission.[49] Copyright 2003, Springer Nature.

Waals forces. Soft templates like biopolymers can be used to synthesize gold nanosponges; one such example of a biopolymer is hyaluronic acid potassium, which can act as a reducing agent and stabilizer, and the soft template was reacted with the gold precursor under hydrothermal conditions to prepare gold sponges.[106] Natural cellulose has also been reported to function as a soft template in the fabrication of TiO_2/Ag nanosponge composites, which have been proven to be low-cost and eco-friendly (Fig. 7c).[107] Walsh et al. reported the synthesis of nanosponge gold, silver, copper oxide, composites of silver/copper and silver/titania using dextran as a sacrificial soft template (Fig. 7d–g).[49] The benefit of adopting the dextran template is that it contains aldehyde groups, which can be leveraged for in situ metal reductions and the nucleation of monodisperse metallic clusters.

Sacrificial templates. In the sacrificial template process, the template is removed while the simultaneous formation of nanostructures is achieved. The template removal does not require any additional step, because it can be removed via galvanic replacement reaction or gradual in situ dissolution during the synthesis process.[108,109] Sacrificial soft templates also have been used to synthesize monometallic gold and silver nanosponges. Khan and coworkers exploited the sol–gel method using a non-ionic surfactant (Triton X-45 and X-100) as the sacrificial template for Ag, Au and CuO nanosponges.[110,111] They reported a series of silver monoliths achieved through Triton X-100 with the inclusion of different additives to tune the surface area favourable for catalysis.[110] Another study conducted by Kwak and co-workers demonstrated the formation of macroporous gold nanosponges by calcination of the metal precursor ($HAuCl_4$) incorporated in the soft agarose template as

shown in Fig. 8a.[112] During calcination, the removal of the template and the sintering of Au nanoparticles present within the pores to form a 3D lining structure occur simultaneously. In accordance with green chemistry principles, Tong et al. proposed a precipitation–sintering process using glucose as the sacrificial template to prepare spongy porous ferrite MFe_2O_4 (M = Fe, Zn, Co, Ni, Mn, etc.).[113] The micro-polyhedral spongy ferrite displayed a homogeneous structure (Fig. 8b–g) and their shape and size-dependent properties could be easily adjusted.

3.2.2 Solution derived. In addition to the template reduction method, kinetically controlled reduction of solution can also yield porous sponge-like nanostructures (Fig. 8h and i). Sodium borohydride reduction is one of the oldest methods for preparing nanoparticles from metal precursors using capping agents but received less attention in synthesizing porous nanostructures. After the first report by Krishna et al. $NaBH_4$ reduction in the absence of capping agents has been demonstrated to be a facile route for preparing nanostructured materials. Noble metals such as Au, Ag, Pd and Pt were prepared through this method, by simply mixing the metal precursors with $NaBH_4$ in a controlled fashion. The strain effect present in nanostructures has been shown to change the activation energy of intermediates when non-metallic elements are added to noble metal catalysts. Motivated by this, Li et al. presented boron-doped silver nanosponges prepared in dimethylformamide solution by the reduction reaction of the Ag precursor and $NaBH_4$. Boron is inserted into the Ag lattices during the reduction process to finally produce a porous structure containing 15 at% boron, which displayed a better nitrogen reduction reaction. This technique is being used to investigate diverse combinations of metals for the preparation of bimetallic
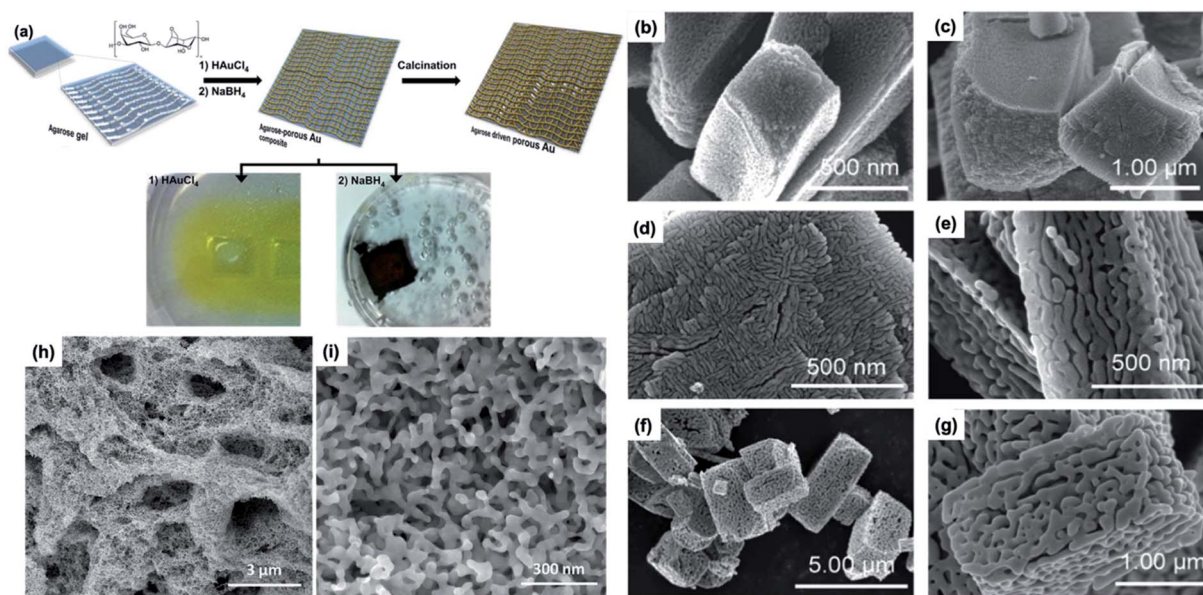
Fig. 8 Sacrificial template synthesis approach for preparing nanosponge structures. (a) Schematic representation of Au sponge preparation using an agarose mixture. Reprinted with permission.[112] Copyright 2021, Elsevier. (b)–(g) FE-SEM images of spongy porous ferrite at different sintering temperatures: (b) 350 °C, (c) and (d) 400 °C, (e) 500 °C and (f) and (g) 700 °C for 5 hours. Reprinted with permission.[113] Copyright 2014, Royal Society of Chemistry. (h) and (i) Low magnification and high magnification FE-SEM images of Au nanosponges, respectively. Reprinted with permission.[53] Copyright 2010, American Chemical Society.

porous structures without any capping agents. Using H_2PtCl_6 and $RuCl_3$ as sources for Pt and Ru, Xiao *et al.* produced PtRu nanosponges by reducing the metal precursors in $NaBH_4$. The presence of Ru improved the surface electronic structure of Pt and the composition of the final product can be altered by changing the ratio between metal precursors.

3.3 Thermal decomposition

Various metallic oxide/sulphide/phosphide nanosponges can be prepared *via* thermal treatment, where metal precursors are decomposed at relatively higher temperatures in the presence or absence of air. After heating for a specific period, the product is then washed and dried to obtain a sponge-like nanostructure.

3.3.1 Hydrothermal. Hydrothermal treatment is a solution-based process, in which heating of aqueous solution above the ambient temperature and pressure results in the formation of nanostructured materials.[114] The general synthesis of alloy structures involves heating of either precursor solution of metal nanoparticles or solution containing the substrate (sponge-like or foam) inside a sealed Teflon autoclave,[115] thus forming a sponge like nanostructure on the surface of the substrate or by interconnection of nanoparticles.[35,116] This method gives precise control over the process parameters, thereby obtaining nanostructures with the desired morphology and composition.[114,117] Nanomaterials that are unstable at high temperature or have high vapor pressure can be prepared by this method with minimal loss, and the final product formed has a uniform size and high crystallinity with outstanding properties.[117,118] Zhang *et al.* presented a self-assembly technique to synthesize gold nanosponges under hydrothermal conditions.[116] The hydrothermal conditions were necessary in removing surfactants from the starting material, *i.e.*, surfactant-capped gold nanoparticles, to form gold nanosponges with finely branched nanowires as shown in Fig. 9a–c. The diameter of these nanowires can be adjusted by controlling the surfactant population, temperature, type of alcohol solution, concentration of nanoparticles, and time. The presence of a binder and additives during the synthesis hinders the surface contact of the electrode/electrolyte, which impairs the electrochemical performance. Therefore, binder-free and additive-free methods are favoured in synthesizing sponge-like electrodes.[119] One-step binder-free synthesis of nickel-based sponge-like nanostructures has also been accomplished by this synthetic approach. For example, Shi *et al.* prepared Ni sponge by the hydrothermal reaction of a mixture of $Ni(CH_3COO)_2 \cdot 4H_2O$ and
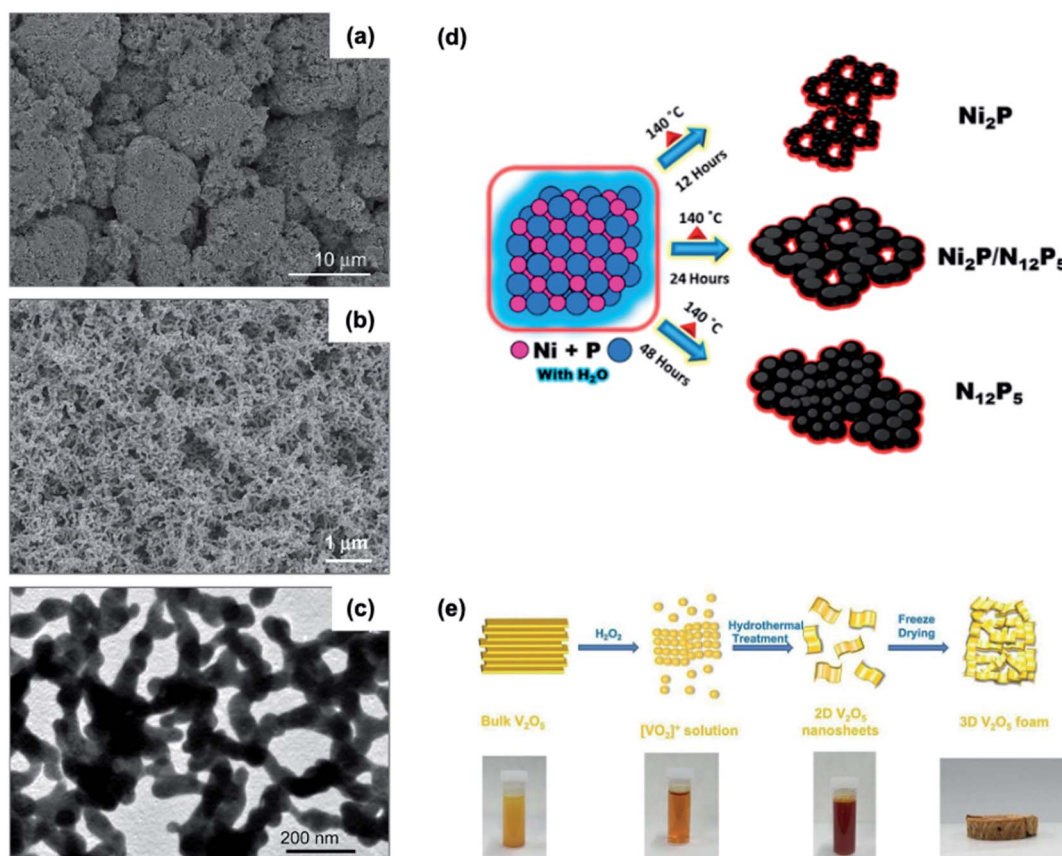
Fig. 9 Hydrothermal synthesis approach for preparing nanosponge structures. Uniform Au sponge images at various magnifications: (a) panoramic FE–SEM image, (b) detailed view of the FE–SEM image and (c) TEM image. Reprinted with permission.[116] Copyright 2007, American Chemical Society. (d) Schematic illustration showing structural and morphological phase transformation of Ni–P at 140 °C at different time periods. Reprinted with permission.[35] Copyright 2018, American Chemical Society. (e) Schematic representation (top) and actual change (bottom) during the synthesis of a V_2O_5 sponge-like material. Reprinted with permission.[122] Copyright 2015, Wiley-VCH.

This journal is © The Royal Society of Chemistry 2022

J. Mater. Chem. A, 2022, **10**, 14221–14246 | **14229**

hydrazine hydrate at 160 °C for 6 h.[119] Nickel phosphides have found numerous electrochemical applications due to their dominant electrical conductivity, high theoretical capacity, physicochemical properties and metalloid character.[120,121] However, the typical synthetic routes to Ni–P are expensive and involve multiple steps to obtain the desire final product.[35] Accordingly, Surendran et al. devised a single-step hydrothermal technique to produce three different crystal structures of Ni–P (Ni_2P, $Ni_2P/Ni_{12}P_5$ and $Ni_{12}P_5$) having an interweaved sponge-like morphology.[35] The hydrothermal treatment was carried at a constant temperature of 140 °C for three different time periods (Fig. 9d); after 12 h (Ni_2P) spherical particles were interconnected with an open sponge-like structure. Upon further increasing the time period to 24 ($Ni_2P/Ni_{12}P_5$) and 48 h ($Ni_{12}P_5$), the porosity decreased significantly because of the agglomeration of individual particles to form bigger particles. In addition to nickel-based sponge structures, the synthesis of vanadium oxide was also possible through the hydrothermal method. Zhu et al. presented a hydrothermal and freeze-drying process to synthesize self-assembled V_2O_5 sponge-like nanomaterials as shown in Fig. 9e.[122]

3.3.2 Solvothermal. The solvothermal process is similar to the hydrothermal process; organic solvents are used instead of water in the former, and the reaction temperature is just above the critical temperature of the solvent. Porous metal oxide nanostructures developed through the solvothermal approach have shown promising results in next generation electrochemical energy storage applications.[123,124] Bi_2SiO_5 nanostructures, which are related to bismuth Aurivillius-phase oxides, have displayed exceptional luminescent and photocatalytic properties.[125] Cheng et al. developed ethylene glycol assisted template-free solvothermal synthesis of 3D sponge-like Bi_2SiO_5 nanostructures at a temperature of 150 °C for 6 h.[125] Lu and co-workers reported low-temperature decomposition of manganese formate to produce sponge-like hausmannite (Mn_3O_4). Large sponge-like structures with crystallographic symmetry can be obtained by simply increasing the reaction time.[126] When compared to metal oxides, metal sulphides present remarkable properties such as large specific capacity, tuneable electronic, optical and chemical properties, minimum redox potential, and enhanced volume expansion.[127] The photoelectrochemical performance of $CuInS_2$ relies on their nanostructure, but the fabrication of 3-D microspheres that show desirable results is still challenging.[128] Using CuCl, $InCl_3$, and thiourea as starting materials, Liu et al. prepared 3D sponge-like $CuInS_2$ microspheres (Fig. 10a and b) via a solvothermal approach at 180 °C for 24 h with the support of poly(-vinylpyrrolidone) as the surfactant.[128] Binary metal sulphides exhibit good electronic conductivity and transport kinetics that can enhance the catalytic activity.[129] A low-cost and facile solvothermal approach described by Chen et al. employed ethylene glycol, sulphur powder, and N,N-dimethylformamide as starting materials to synthesize sponge-like NiS/Ni_3S_2 hybrid nanosheets on Ni foam as illustrated in Fig. 10c.[130] Using a silane coupling agent (SCA) has been explored to alter the material surface for the development of new functional materials.[131,132] Fan et al. described the synthesis of nanocrystalline Ag_2S and Ag by applying the SCA-based solvothermal approach, followed by thermal processing in a N_2 atmosphere.[133] SCA controlled the size of Ag_2S and Ag crystals to form small nanoparticles, thus avoiding the aggregation and to maintain a good dispersion by forming a thin shell. Scanning electron microscopy revealed that a sponge-like structure covers the Ag_2S nanoparticles and that prolonged thermal treatment would reduce the sponge
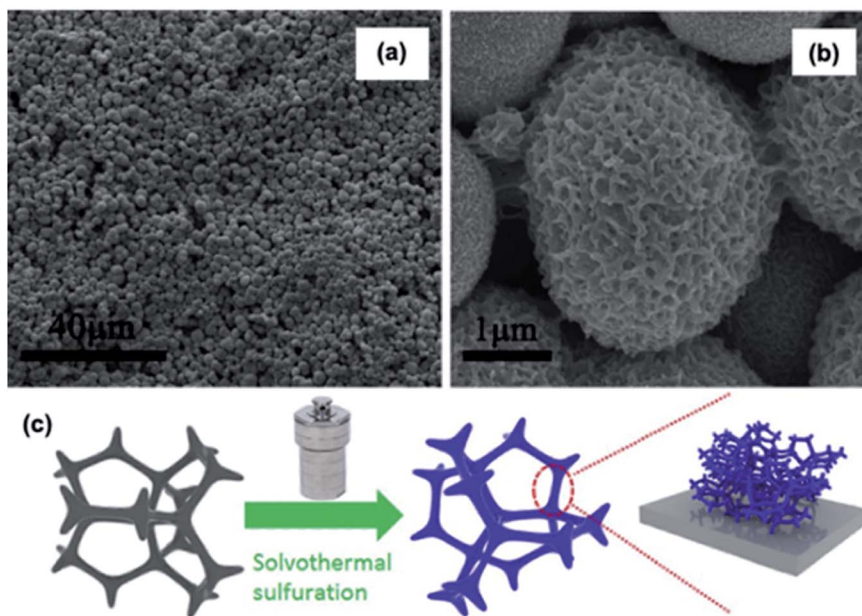
Fig. 10 Solvothermal synthesis approach for preparing nanosponge structures. SEM images of $CuInS_2$ microspheres: (a) low magnification and (b) high magnification. Reprinted with permission.[128] Copyright 2014, American Chemical Society. (c) Schematic representation of the solvothermal process to prepare NiS/Ni_3S_2 hybrid nanosheets on Ni foam. Reprinted with permission.[130] Copyright 2018, Elsevier.

14230 | J. Mater. Chem. A, 2022, **10**, 14221–14246

This journal is © The Royal Society of Chemistry 2022

structures. The synthesis of an In_2S_3 low dimensional structure by the hydrothermal approach is difficult because of self-aggregation. Hence, Kumar *et al.* developed a direct solvothermal method to produce 2D sponge-like In_2S_3 nano-flakes.[134] The In_2S_3 electrode was made by heating nickel foam with precursor solution, containing indium nitrate, thiourea, isopropyl alcohol and deionized water, at 180 °C for 24 h. Although metal sulphides have found recognition in various applications, metal oxides are more preferable because of low cost, low dimensions, high sensitivity and simple integration.[127] Hydrothermal and solvothermal methods are most commonly explored, but other approaches such as sintering,[135,136] calcination[137] and pyrolysis[138,139] have also been explored.

3.4 Electrodeposition

Electrodeposition is another versatile technique, where the material is deposited controllably from the electrolyte solution onto a substrate by applying high voltage; the voltage creates high electrostatic force resulting in the formation of accelerated charged droplets to deposit (Fig. 11a).[140,141] The electrochemically fabricated electrode materials have shown good capacity retention, good cyclability, low cost, and environmental friendliness.[142,143] Alloyed nanostructures can also be obtained by mixing different metallic salts in the electrolyte solution.[142] Furthermore, the growth rates can be adjusted by optimizing current density, salt concentration, pH, additives, and deposition temperature.[144] Using electrodeposition, various single and multi-component 3D nanostructured materials can be synthesized with porous structure, dense, fractal-like, sponge-like and cross linked morphologies.[141] Li and Wang mentioned that sponge-like structures display good mechanical strength due to narrow pore size distribution and high porosity that can handle volume change.[141] With increased accessibility of active sites by the electrolyte and large surface area network, the ion transport properties are higher compared to other nanostructures.[141] The synthesis of sponge-like nickel hydroxide ($Ni(OH)_2$) nanostructures by the electrodeposition approach has been widely studied for supercapacitor applications because of low cost and better electrochemical redox activity.[145,146] Jin *et al.* reported the fabrication of a porous sponge-like $Ni(OH)_2$–NiF_2 composite film by anodization of the electrolyte containing a mixture of 1 weight% (wt%) NH_4F and 80 wt% H_3PO_4 at a potential of 3.5 V.[146] The thickness of the film was directly controlled by regulating the anodization time. A similar report on electrodeposition of $LiMn_2O_4$ thin film electrodes by Shui *et al.* discussed that the sponge-like structure demonstrated superior performance to dense structures because of high porosity and mechanical, thermal and chemical stability with a narrow pore size distribution and better transport characteristics.[147] The use of nickel foam as an electrodeposition substrate has allowed the development of a variety of metallic sponge-like structures.[148,149] The article reported by Hu *et al.* described the synthesis of sponge-like ε-MnO_2 with interconnected flakes on a Ni foam substrate (Fig. 11b–e). The electrodeposited samples were further annealed under different conditions.[148] The electrolyte was composed of a mixture of manganous acetate and sodium sulphate, and the electrodeposition was performed in a three-electrode setup at a current density of 5 mA cm^{-2}. Moreover, it was observed that, at lower temperatures, isolated spheres were formed on the surface of the deposited layer and, at higher temperatures, more cracks were formed. Yang *et al.* developed edge-oriented sponge-like MoS_2 films by anodising Mo foil in electrolyte solution containing a mixture of oxalic acid, Na_2SO_4 and NaF at a constant current density of 25 mA cm^{-2} in a two-electrode system.[150] To convert the Mo oxide films into MoS_2 films, a reaction with sulphur in a chemical vapour deposition furnace followed after anodizing.

In recent years, the evolution of hydrogen bubbles as a dynamic template has been utilized in electrodeposition of porous nanostructures.[151,152] The reduction of H$^+$ resulted in the formation of hydrogen bubbles and the porous structure contained small grains with ramified walls (Fig. 12a).[151] The synthesis of transition metal phosphides for electrocatalysis usually requires a high temperature and complex process. Park *et al.* reported a low cost and one-step electrodeposition method of Cu–Co–P porous foam using a hydrogen bubble template.[66]
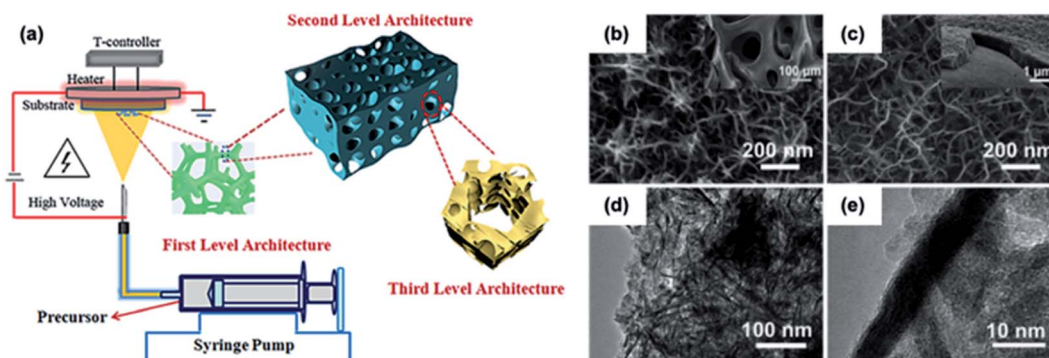
Fig. 11 Electrodeposition synthesis approach for preparing nanosponge structures. (a) Schematic representation of the electrochemical deposition technique to prepare 3D porous Li_3VO_4 (LVO) and carbon-coated Li_3VO_4 (LVO@C) on a Ni-foam disc. Reprinted with permission.[149] Copyright 2018, American Chemical Society. (b) SEM image of ε-MnO_2 electrodeposited at 35 °C; inset figure shows pristine Ni foam. (c) SEM, (d) TEM and (e) HRTEM images showing ε-MnO_2 annealed at 350 °C for 15 hours. (b)–(e) Reprinted with permission.[148] Copyright 2014, Royal Society of Chemistry.

This journal is © The Royal Society of Chemistry 2022

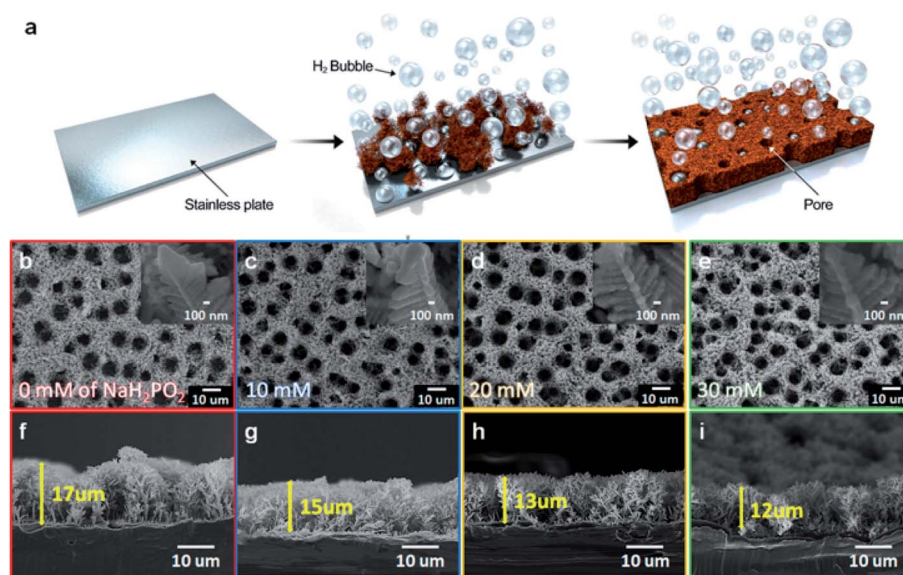*J. Mater. Chem. A*, 2022, **10**, 14221–14246 | **14231**

Fig. 12 Hydrogen bubble template synthesis approach for preparing nanosponge structures. (a) Schematic representation of the synthesis of Cu–Co and Cu–Co–P$_x$ foam using hydrogen bubbles as a dynamic template. (b)–(i) SEM images of Cu–Co and Cu–Co–P$_x$ foam (top) and their cross sections (bottom) at different concentrations of NaH$_2$PO$_2$ through the electrodeposition process. Reprinted with permission.[66] Copyright 2019, American Chemical Society.

The electrolyte was composed of CuSO$_4$, CoSO$_4$, NaCl, H$_2$SO$_4$, and NaH$_2$PO$_2$, and H$_2$SO$_4$ functioned as a source for the hydrogen bubble template. The Cu–Co–P$_x$ (x is the concentration of the P source) foams were deposited onto stainless steel foil at a current density of 2 A cm^{-2} and concurrently hydrogen bubbles were formed at the electrode surface resulting in porous foam-like nanostructure (Fig. 12b–i). Choi *et al.* prepared a unique sponge structure with a nanodendritic wall and micropore network containing Cu–Co oxide core–shell hybrid nanobranches.[153] The sponge structure was created by using electrodeposition and hydrogen gas evolution at the same time, followed by anodic oxidation and thermal dehydration to get the final nanostructure. Altogether, the electrodeposition process offers a numerous advantages such as low-cost, low-temperature, easily tuned morphology, and high deposition rate due to electric field.[141] Additionally, the electrodes can be synthesized without any additional binder or conductive agents, which directly increases the energy density in batteries.[141,154]

3.5 Miscellaneous methods

In addition to the methods discussed above, a variety of novel methods were also reported for the fabrication of nanosponges. Lang *et al.* employed a supercritical fluid reactive deposition (SFRD) method to prepare a PtCuO/CeO$_2$ catalyst supported on α-alumina sponges (Fig. 13a) that demonstrated good activity for preferential oxidation of CO in the presence of excess hydrogen.[155] Pt and Cu metal–organic complexes dissolved in supercritical CO$_2$ are adsorbed on ceria coated sponge followed by *in situ* reduction in the same state. CO$_2$ was vapourised and eliminated along with residual hydrogen and an organic ligand after the pressure was reduced. Since there is no disturbance of capillary pressure and gravitation, the yield results are uniform

metallic nanoparticles on complex structures with fine pore size. Materials prepared *via* the SFRD method presented nearly two-fold catalytic activity compared to that of wet-chemical impregnation with copper. The increase of catalytic activity was due to the high dispersion of copper on the ceria layers.

Cavitation bubbles generated by high-intensity ultra-sonication are referred to as microreactors because they provide high pressure and temperature to initiate the formation of active molecules in dissolved molecules.[156] Skorb and coworkers described the high-intensity ultrasonication treatment of aluminium nickel alloy dispersion in an aqueous medium (Fig. 13b).[156,157] During the ultrasonication of the initial Al/Ni alloy (Al$_3$Ni$_2$ and Al$_3$Ni intermetallides), aluminium is converted to the oxide form with nickel achieving a metallic state by reduction. As a result, a sponge-like nanostructure was formed with the modified surface of aluminium and active nickel centres dispersed in the matrix.[157] Since the Al/Ni catalyst system (sonogenerated metal oxides and presence of metallic Ni) is sonoactivated, it does not require pre-activation to show efficient catalytic performance.

Syubaev *et al.* presented a scalable nanosecond (ns)-laser ablation method combined with advanced chemical processing of thin silica glass supported Au films to prepare 3D plasmonic nanosponges as shown in Fig. 13c.[158] Firstly, using a custom made magnetron sputtering system with three discharge gases (Ar, N and purified air) Au films are deposited on the silica glass substrate without any adhesive sub-layer. Next, the nitrogen rich Au films are precisely ablated using ns-laser pulses generated from a Nd:YAG laser system to create parabolic nanobumps having a perforated nanostructure on the inside surface (Fig. 13d–f). Moreover, the porous nanostructure beneath the surface of the nanobumps can be revealed by gently
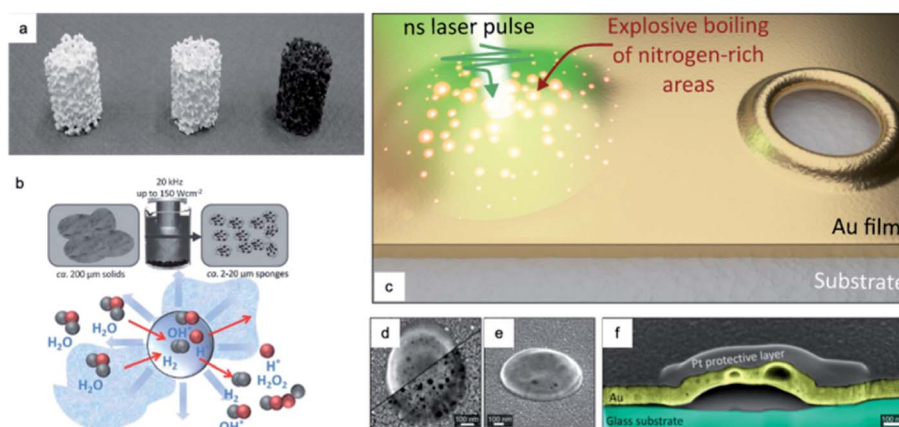
14232 | *J. Mater. Chem. A*, 2022, **10**, 14221–14246

This journal is © The Royal Society of Chemistry 2022

Fig. 13 Miscellaneous approaches for preparing nanosponge structures. (a) Left to right shows the preparation of the catalyst at three different stages, starting as blank α-Al_2O_3 to coating with CeO_2 and subsequent calcination. Reprinted with permission.[155] Copyright 2011, Elsevier. (b) Schematic representation of the synthesis of sponge like materials through ultrasound (top) and formation of active species during cavitation bubble collapse by water sonolysis. Reprinted with permission.[156] Copyright 2013, Royal Society of Chemistry. (c) Schematic representation of direct laser printing to prepare nanosponge structures on a glass supported Au film. (d) and (e) SEM images of an isolated laser printed nanosponge from top and side views respectively. The two parts of the top view at different e-beam acceleration voltages reveals nanopores beneath the nanobump surface. (f) False colour SEM image of a cross section of the nanobump. (c)–(f) Reprinted with permission.[158] Copyright 2020, MDPI.

etching with an Ar-ion beam to form functional 3D plasmonic nanosponges.

4. Electrochemical energy applications

4.1 Rechargeable batteries

Batteries have become ubiquitous in recent years, leading to developments in electrical energy storage. Their high performance has enabled applications including wearable and portable electronics, smart textiles, electric vehicles and the internet of things (IoT) as well as energy storage from intermittent sources. However, it is essential to discover new chemistry and nanostructured materials for batteries with increased capacity and energy density.

4.1.1 Lithium batteries. Since commercialization, lithium-ion batteries (LiBs) have evolved considerably with unmatched high energy and power density in diverse applications. Present day LiBs are composed of a Li transition metal oxide (cathode) and graphite (anode) that operate reversibly *via* Li-ion intercalation. Nevertheless, there is a growing demand for high-energy-density electrodes for LiBs. Nanosponge structures make an excellent choice for improving the cathode and anode performances.[141,159] Their interconnected channels and nanosized pore walls facilitate rapid ion transfer. They can also allow for strain relaxation during charge/discharge cycles.

LiB anode. There is great research interest to study a variety of nanosponge materials as anode materials for LiBs. Mesoporous Au having a large surface area, high conductivity, and low voltage for Au–Li alloying/dealloying shows suitable features for LiB anodes.[160] Thin films of mesoporous Au sponges with interconnected channels and pores of 5–20 nm diameter were used for LiBs anodes. The alloying (0–0.25 V) and dealloying

(0.15–0.45 V) voltages of Au sponge were much lower than those of the Li–Sn alloy, but were comparable to those of thin, solid Au anodes. However, the multilayer mesoporous Au displayed better discharge capacities and cycling stability than the thin, solid gold film (Fig. 14a). The results suggested that the synthesis method might have an influence on the capacity of mesoporous Au, with multilayer mesoporous Au outperforming single-layer mesoporous Au after 30 cycles.

Metal oxides are most prevalent as negative electrodes for LiBs, owing to their high capacity and long cycle life.[24] Morphology controllable 3D conductive oxides such as fluorinated tin oxide (FTO) have a large surface area and interconnected pores extending in all three directions.[161] The galvanostatic cycling process indicates that porous FTO exceeds pure SnO_2 as an anode in terms of cycling retention and storage capacity. In particular, the capacity of the FTO anode remained nearly 600 and 400 mA h g^{-1} after 40 and 50 cycles, respectively. The reported capacity of pure SnO_2 nanobeads is less than 400 mA h g^{-1} after 40 cycles. The superior performance of FTO was associated with the large surface area and integral porous structure that can withstand significant volume change during Li insertion/extraction. Furthermore, the porous voids promote electrochemical contact and diffusion between the internal surface of the oxide and electrolyte, consequently lessening the Li diffusion resistance. Choi et al.[135] and Yuan et al.[162] independently reported sponge-like cupric oxide (CuO) by employing different approaches and investigated their performances as anode electrodes for LiBs. Commercial CuO possesses high theoretical capacity, chemical stability, environmental friendliness, and low cost.[162] However it suffers from electrical contact reduction and electrode pulverisation during the cycling process leading to poor cyclability and rate performance. The as-prepared sponge-like CuO displayed better rate performance,
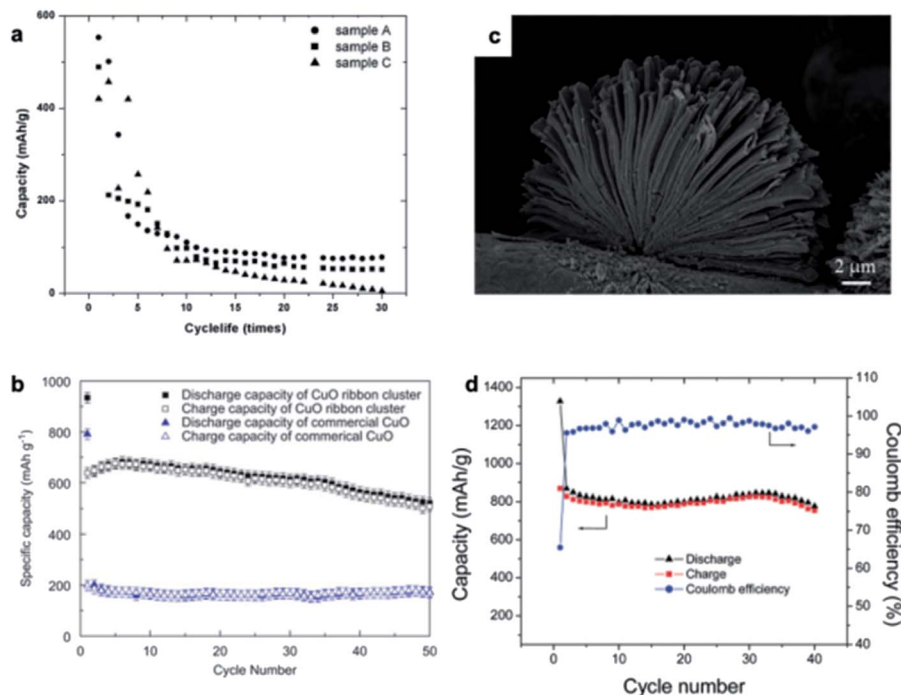
This journal is © The Royal Society of Chemistry 2022

J. Mater. Chem. A, 2022, **10**, 14221–14246 | **14233**

Fig. 14 Electrochemical performances of nanosponge materials as an anode electrode for LiBs. (a) The specific charge capacity *vs.* cycle life of various samples of mesoporous Au. Reproduced from permission.[160] Copyright 2007, IIETA. (b) Comparison of cycling charge and discharge curves between CuO ribbon clusters and commercial CuO at 0.2C. (c) SEM image of CuO ribbon clusters when charged after 50 cycles. (b) and (c) Reprinted with permission.[162] Copyright 2012, Elsevier. (d) Cycling charge and discharge capacitance performances and coulombic efficiency of Mn_3O_4 at 0.25C. Reprinted with permission.[163] Copyright 2011, American Chemical Society.

stability, and specific capacity than the commercial CuO anode (Fig. 14b). The discharge capacity of sponge-like mesoporous CuO ribbon clusters (Fig. 14c) at a current rate of 0.5C was found to be 572 mA h g^{-1} after 10 cycles and slowly reduced on increasing the current rate (485, 394, 285, and 206 mA h g^{-1} at 1, 2, 3 and 4C, respectively).[162] When the current rate returned to the initial value, high discharge capacity (430 mA h g^{-1}) with high retention capacity (77%) was recorded, which was superior to that of commercial CuO (120, 51, 22, 16, 15 and 96 mA h g^{-1} at 0.5, 1, 2, 3, 4 and 0.5C, respectively). Unique mesoporous ribbon clusters and small CuO nanocrystals expedite the Li-ion diffusion and the large surface specific area provides more reaction sites. The increased electrochemical kinetics is due to the good electrical conductivity originating from the rigid connection of nanocrystals. This nanostructure can considerably enhance the cyclability of the CuO anode material. The 3D sponge structure of CuO nanoparticles also presented high capacity (674 mA h g^{-1}) and excellent rate capability compared to CuO/CuO-composite anodes.[135] The 3D network structure with porous and secondary particles was responsible for the better performance.

On the other hand, manganese is naturally more abundant, less harmful, and cheaper than Co, and therefore it is of great interest to study manganese-based anode materials. In this regard, Gao *et al.* prepared sponge-like nanosized Mn_3O_4 by a simple precipitation method and analysed for LiBs anodes.[163] The initial charge capacity (869 mA h g^{-1}) is almost equal to the theoretical capacity of a fully reversible conversion reaction and

greater than that of conventional graphitic carbon. The charge–discharge profiles demonstrate that Mn_3O_4 can deliver high reversible capacity close to 640 and 500 mA h g^{-1} at a current rate of 2.5C and 10C, respectively. Moreover, the coulombic efficiency is greater than 65% for the first cycle and almost 95% for the subsequent cycles (Fig. 14d). Mn_3O_4 shows lower working voltages (0.6 V for reduction and 1.6 V for oxidation), and thus full cells operating at a higher voltage with higher energy density can be obtained by combining a suitable cathode. These performances are due to the porous sponge structure that allows for rapid Li ion shuttle; the large surface area maximizes the utilization of active material. The remarkable architecture can also withstand volume change-induced strain during the charge/discharge process while maintaining the electrode integrity.

Lithium (Li) metal is one of the most promising anode materials, with ultralow electrochemical potential (−3.04 V *vs.* SHE) and high specific capacity (3861 mA h g^{-1}), making it an ideal choice for future high energy density rechargeable batteries.[164,165] However, uneven Li nucleation and inconsistent solid electrolyte interphase (SEI) formation during the charging/discharging process can result in uncontrolled Li dendrite growth, posing safety concerns and capacity deterioration.[164,166] The construction of 3D nanostructures that can host Li metal can alleviate the above difficulty by offering a broad surface area and homogeneous Li deposition.[167] In this context, Li *et al.* proposed a conductive-dielectric gradient sponge capable of top-down Li dissolution and bottom-up Li

14234 | *J. Mater. Chem. A*, 2022, **10**, 14221–14246

This journal is © The Royal Society of Chemistry 2022

deposition, resulting in a stable dissolution/disposition mechanism.[167] The as-prepared Li metal anode exhibited a long cycle life of 740 h at 1 mA cm^{-2} when tested on a symmetric cell and displayed 95.6% coulombic efficiency at 8 mA cm^{-2}. The increased performance has been ascribed to the synergistic effect of uniform Li$^+$ distribution in the dielectric part and decreased local current in the conductive element, causing reduced dendrite growth and volume change. Furthermore, when assembled as a full cell with a commercial LiFePO$_4$ cathode, the conductive-dielectric gradient sponge demonstrated better rate and cycle performance.

LiB cathode. As discussed above, similar findings have also been demonstrated in cathode materials for LiBs. Mesoporous Li-based layered and spinel structures have better rate capability and excellent cyclability compared to their bulk counterparts.[168] Thin films of spinel LiMn$_2$O$_4$ sponge-like structures developed *via* electrospray deposition were tested as cathode materials of 2032 coin-cells with lithium as an anode material.[147] The charge–discharge curves of the cell suggest a reversible Li insertion/extraction process into LiMn$_2$O$_4$ at 4 V. The cell does not show significant capacity fading over the next 50 cycles. The sponge-like structure exhibited better electrochemical characteristics such as rate capability and cell resistance than other fractal-like porous and dense structures. The low charge transfer resistance in the sponge-like structure came from the large interface between the active material and electrolyte. The impendence spectra of sponge-like LiMn$_2$O$_4$ further revealed a decrease in charge transfer resistance with an increase in film thickness. Among the other cathode materials, vanadium based oxides are also researched as promising materials owing to their high specific capacity, low cost, and their abundance.[169,170] Various low-dimensional nanostructures of V$_2$O$_5$ such as nanoribbons, nanosheets, and nanorods have shown better performance than the bulk structures.[159] However, due to pulverization and self-aggregation, their rate performance and cyclability were poor. 3D hierarchal porous sponge-like V$_2$O$_5$ micro/nanostructures (V$_2$O$_5$-SLMNS) can exhibit better electrochemical performances than low-dimensional V$_2$O$_5$ nanostructures, ascribed to the large surface area, rich in pores and conductive networks.[159] Electrochemical characterization using coin type cells indicate that V$_2$O$_5$-SLMNS (232 mA h g^{-1}) show superior second discharge specific

capacities than V$_2$O$_5$ nanoribbons (190 mA h g^{-1}) (Fig. 15a). The cycling stability of V$_2$O$_5$-SLMNS (87%) was also better than that of V$_2$O$_5$ nanoribbons (69%) after 50 cycles at a current density of 100 mA g^{-1}.

Li-S anode. Li-S batteries (LSBs) are regarded as a next-generation energy storage system due to their higher specific energy and cost lower than LiBs.[171] The shuttle reaction originating from soluble polysulfide intermediates, combined with the insulating nature of sulphur and Li$_2$S, and large volume expansion hinder their practical applications. A stable Li metal-based anode has been studied to tackle the above issues. Spray quenching Li metal on the 3D sponge nickel (SN) matrix can function as a flexible anode (SEI@Li/SN) and dendrite inhibitor.[172] A steady overpotential within 75 mV for 1500 h benefiting from the combined qualities of the *in situ* formed SEI and 3D lithophilic SN matrix was recorded at 5 mA cm^{-2}/10 mA h cm^{-2}. When assembled as a LSB, the full cell exhibited high discharge capacity (785 mA h g^{-1}) and high capacity retention (99.82%). After 200 cycles, the surface morphology of the SEI@Li/SN anode remained unchanged without dendrite cluster overgrowth (Fig. 15b). Furthermore, the full cell delivered uniform polarisation values for different mechanical deformation conditions. The *in situ* modified SEI layer at the anode and suitable lithium polysulfide absorbent at the cathode (such as Ni$_3$S$_2$) can improve the overall structural conductivity leading to improved electrochemical performances. Li–boron (B) alloys (Li–B) are of great interest in LSBs because of their competence to suppress the dendrite formation, enhancing the cyclability and decreasing the interface impedance.[173] Zhang *et al.* demonstrated that the Li–B alloy with excess Li integrated with a Li$_7$B$_6$ loofah sponge-like structure can replace the Li metal anode in LSBs.[174] Through 100 cycles, the deposition/dissolution efficiency of the Li–B alloy remained remarkably consistent (Fig. 15c). The unique morphology of the Li–B alloy further confines the growth of Li dendrites and crack formation that substantially improved safety and cyclability. An increase in the Li$_7$B$_6$ component could expedite SEI layer formation by reducing the current density. Additionally, the sponge structure withstood volume change or potential deformation during the cycling process.

LiO$_2$ cathode. Li–air batteries provide the highest theoretical energy density compared to other storage technologies.[175] In
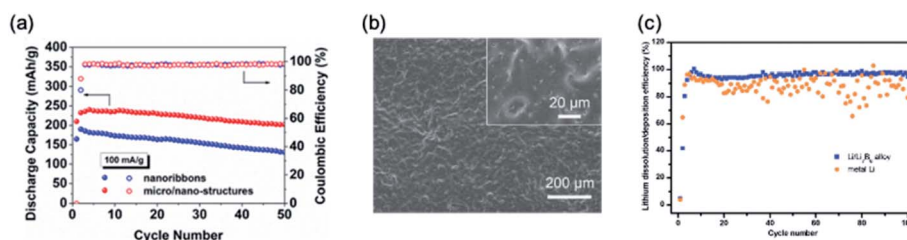
Fig. 15 Electrochemical performances of nanosponge materials as electrodes for Li-based batteries. (a) Comparison of the cycling performances of V$_2$O$_5$-SLMNS and V$_2$O$_5$ nanoribbons at 100 mA g^{-1}. Reproduced with permission.[159] Copyright 2018, Elsevier. (b) SEM images of a solid electrolyte interface at the Li/SN anode of a Li–S battery. Reproduced with permission.[172] Copyright 2020, Wiley-VCH. (c) Comparison of cycling efficiency between the Li–B alloy and Li metal as anode electrodes for a Li–S battery. Reproduced with permission.[174] Copyright 2014, Royal Society of Chemistry.

general, they are composed of oxygen (cathode), Li metal (anode) and a Li⁺ conducting electrolyte.[175,176] Self-supporting sponge-like ε-MnO$_2$/Ni can function as an excellent cathode without the need for an additional binder or conductive agents for Li oxygen batteries.[148] At a current density of 500 mA g⁻¹, the hybrid sponge structure displayed high discharge capacity close to 6300 mA h g⁻¹ without controlling the discharge depth. In addition, stable capacity greater than 1000 mA h g⁻¹ was observed over 120 cycles with slight fading at the beginning and better retention of the initial morphology (Fig. 16A). The presence of excess vacant sites of oxygen in ε-MnO$_2$/Ni contributed to higher activity. As a result of heat treatment, the adhesion between ε-MnO$_2$ and Ni foam was increased, consequently enhancing the electrical conductivity, and reducing the electrochemical impedance. All these conditions favoured the rapid reversible formation/deformation of insulating Li$_2$O$_2$ resulting in high cycling stability of LiO$_2$ batteries.

4.1.2 Non-lithium batteries

Sodium-ion battery cathode. Sodium (Na)-ion batteries (NiBs) have made significant progress in recent years and are viable options because they are made from raw materials that are cost efficient, more abundant, and less harmful.[177,178] LiBs and NiBs share a similar battery architecture and manufacturing process which can accelerate their development models. To match the performance of LiBs, many challenges need to be overcome by NiBs such as sluggish solid-state diffusion due to the relatively larger size of Na⁺ compared to Li⁺ that may result in poor energy efficiencies. The higher negative redox potential of Na relative to Li can cause low cell voltages, and consequently low energy density. A large number of vanadium (V) based cathodes, including oxides, phosphates, polyanions and bronzes, have been studied for NiBs mainly due to their good electrochemical interaction with Na⁺, high energy density, and capacity.[179] A

sponge-like V$_2$O$_5$ cathode at a current density of 20 mA g⁻¹ delivered a specific discharge capacity of 216 mA h g⁻¹ for NiBs.[122] At 100 mA g⁻¹, the electrode was able to retain about 73% of initial capacity after 100 cycles. This high output was attributed to the largely exposed facet (001) and large spacing between the layers that provides short diffusion paths. Moreover, the spongy structure derived from the self-assembly of nanosheets can tolerate high pressures and can significantly absorb electrolytes. Li *et al.* assessed the electrochemical performance of Na$_3$V$_2$(PO$_4$)$_3$ with different morphologies such as porous sponge-like, plate-like and irregularly shaped.[180] Among them, the sponge-like structure could achieve a high initial capacity of 101.77 mA h g⁻¹ at 30C after 700 cycles. The open 3D architecture of the sponge facilitates ion diffusion and the large surface provides more access to the electrolyte as shown in Fig. 16B.

Zn-based battery anode. Zinc anodes are widely used in alkaline batteries that provide good energy density by using water-based electrolytes and abundant and inexpensive electrode materials. However, under standard recharging conditions, zinc tends to grow into needle-like dendrite structures on the electrode surface that can cause a short circuit. Parker and coworkers have explored Zn sponges for Zn-based batteries including Ni–Zn cells,[181,182] Zn–air cells[183] and rechargeable alkaline Zn batteries.[184] Zn sponge and rechargeable nickel hydroxide (NiOOH) as the anode and cathode, respectively, were assembled for nickel–zinc (Ni–3D Zn) cells. This combination resulted in high energy densities and life cycles that matched/ exceeded the performance of LiBs, while only relying on benign and inexpensive materials.[182] Benefitting from the sponge structure, the Zn anodes did not show significant dendrite formation even under extreme power load conditions. Besides that, they could handle up to 5400 charging and

Fig. 16 Electrochemical performances and schematics of nanosponge materials as electrodes for batteries. (A) Cycling performance of a 60 h@350 °C ε-MnO$_2$/Ni electrode at 500 mA g⁻¹. Reproduced with permission.[148] Copyright 2014, Royal Society of Chemistry. (B) Schematic representation of the sponge-like porous Na$_3$V$_2$(PO$_4$)$_3$ electrode. Reproduced with permission.[180] Copyright 2016, Elsevier. (C) Cycling performance of Ni–3D Zn coin cells at 4000 cycles and 54 000 cycles. (D) Microscopic image of Zn sponge after ~54 000 cycles revealing a nominal change in the shape and no dendrite growth. Reproduced with permission.[182] Copyright 2017, American Association for the Advancement of Science.

14236 | *J. Mater. Chem. A*, 2022, 10, 14221–14246

This journal is © The Royal Society of Chemistry 2022

discharge cycles with the duty cycle of start–stop batteries, which need powerful pulses but minimum zinc usage (Fig. 16C and D). When tested for Zn–air cells, the Zn sponge anode delivered 740 mA h g^{-1} discharge capacity which is greater than 90% of theoretical capacity of Zn.[183] The low cell resistance stems from the wired network of metallic Zn at the inner core that reveals long range conductivity with an even current distribution.

4.2 Supercapacitors

Supercapacitors (SCs) should handle rapid charge/discharge rates at high current densities. SCs store opposite charges at the interface of electrolyte/electrode by physisorption, and hence display fast ion kinetics. Nickel appears to be the most prominent transition metal in supercapacitor applications because of its prevalence in nature, low cost, and affinity for rich valence states ($Ni^0/Ni^{2+}/Ni^{3+}$). In an arresting divalent state, Ni metal ions can quickly form compounds of hydroxides, oxides, sulphides, and phosphides and their sponge structures have been reported to have excellent supercapacitor applications.[35,145,185] Ren *et al.* reported that binder-free sponge-like $NiCo_2S_4$ nanosheets with ultra-high mass loading (18.7 mg cm^{-2}) supported on Ni foam (NF) have rich active sites, shorter diffusion channels, and a large area.[185] The supporting NF can function as a current collector that considerably decreases the resistance and improves the ion kinetics. Additionally, the ultra-high loading allows for more active sites for energy storage per unit area. The $NiCo_2S_4$–NF hybrid electrode at 15 mA cm^{-2} could reach a high area capacity of 11.97 F cm^{-2}. The corresponding asymmetric supercapacitor attained a high area energy density (0.47 mW h cm^{-2}) and power density (6.59 mW cm^{-2}) for 5000 cycles with good capacity retention (80.1%) (Fig. 17a). A highly porous sponge-like $Ni(OH)_2$–NiF_2 composite (PNC) achieved better specific capacitance (2090 F g^{-1} at 10 mV s^{-1} and 1218 F g^{-1} at 200 mV s^{-1}) than reported Ni based electrodes.[186] The study also presented excellent cycling stability and rate capability (>1200 F g^{-1} after 2000 cycles). VO_2/TiO_2 nanosponges with a precisely controlled nanostructure and composition as binder-free electrodes show excellent results for supercapacitors.[154] The synergistic effect of stable TiO_2 and high-capacity VO_2 tolerated the large volume change, and interconnected pores offered more voids and defects, yielding

more active redox reaction sites, which led to a high capacity of ~548 F g^{-1} at a scan rate of 10 mV s^{-1} of VO_2/TiO_2 nanosponges and a retention of about 84.3% even after processing for 100 cycles. The voids in the Mn-based oxide structure offer increased active sites and high capacity for intercalation of ions, making them promising electrode materials. Li *et al.* investigated sponge-like mesoporous Mn_3O_4 as a supercapacitor electrode in a 1 M Na_2SO_4 electrolyte and demonstrated high specific capacity with improved cycling performance and stability.[187] Even after 5000 cycles, a high capacity retention close to 99% at a current density of 2 A g^{-1} was maintained. The desirable performance was attributed to the unique sponge structure with a high specific area and 3D micro-network (Fig. 17b and c). Bismuth oxides, non-poisonous and inexpensive, have also been studied in various electrochemical domains. By employing the wet chemical process, Shinde *et al.* evaluated polycrystalline and mesoporous bismuth oxide (Bi_2O_3) for supercapacitor electrodes.[188] Bi_2O_3 had a micro-sponge-ball-like structure with upright standing petals separated by crevices with large surface areas. This peculiar nano-architecture facilitated rapid ion transfer through short diffusion routes that resulted in a high specific capacity of 912 F g^{-1} at 2 A g^{-1}. Meanwhile, the asymmetric supercapacitor assembly of Bi_2O_3 and graphite could function without fluctuations over 5000 cycles at 2 A g^{-1} with a retention of over 80%, denoting the chemical stability and robustness of Bi_2O_3 sponge balls.

4.3 HER

Hydrogen production technologies like thermolysis, photolysis, and biomass are relatively expensive and consume more energy than the energy obtainable by produced hydrogen. On the other hand, water electrolysis does not release any greenhouse gases and is much cheaper compared to other hydrogen production technologies. Water splitting technology can be used to split H_2O into H_2 and O_2 by passing current at a required potential. Various noble metal-free and inexpensive materials have been investigated to obtain a water splitting electrocatalyst and minimize the overpotential required to split the H_2O molecule. The tunable porosity and unique electronic properties make nanosponge materials a potential candidate as electrocatalysts in the hydrogen evolution reaction (HER). Several nanosponge
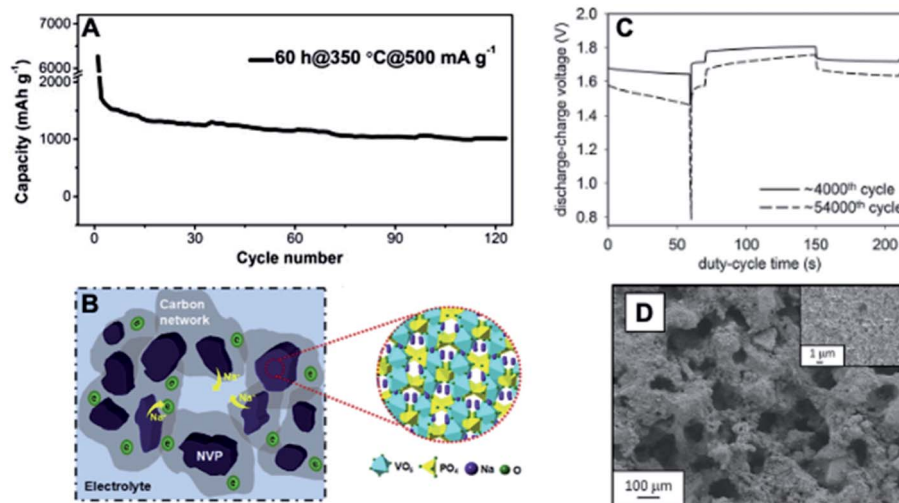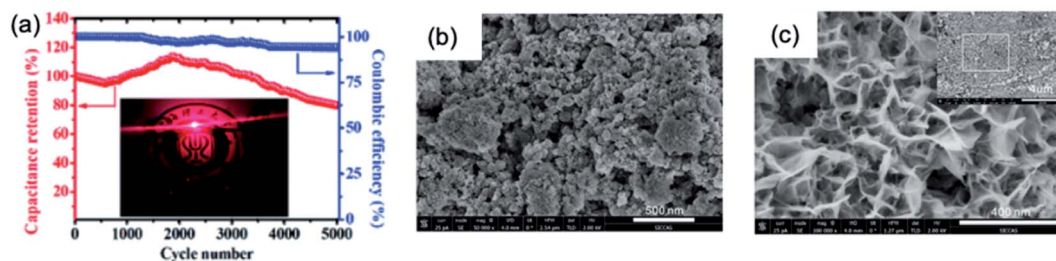

Fig. 17 Electrochemical performances and schematics of nanosponge materials as electrodes for supercapacitors. (a) Cycling performance and efficiency of $NiCo_2S_4$–NF as an asymmetric supercapacitor; inset shows two asymmetric supercapacitors connected in series to illuminate a LED. Reproduced with permission.[185] Copyright 2021, Royal Society of Chemistry. (b) and (c) FESEM images of Mn_3O_4 electrodes before and after cycling for 5000 cycles, respectively. Reproduced with permission.[187] Copyright 2017, Elsevier.

This journal is © The Royal Society of Chemistry 2022

J. Mater. Chem. A, 2022, **10**, 14221–14246 | **14237**

electrocatalysts have been constructed using inexpensive metal-based materials for overall water splitting. One such nano-sponge material is a Cu-rich core and Co-rich shell phosphide foam electrocatalyst that presented excellent HER activity and prominent stability, with an overpotential of 138 mV at 10 mA cm^{-2} (Fig. 18a) and small Tafel slope of 48 mV dec^{-1}.[189] According to this study, as the amount of phosphorus was increased in the Cu–Co–P foams, the pore numbers, the electrochemical surface area (ECSA), and HER activity were remarkably enhanced. This improved HER activity was attributed to the charge separation between the negatively charged P ($\delta-$) and positively charged Cu and Co ($\delta+$). Moreover, this remarkable HER performance can be understood by a phenomenon that as the concentration of anions is increased (phosphide in this case), the positively charged metal cation gets converted to its highest oxidation state and acts as an active site for accelerated water electrolysis. Sulfide/phosphide-mediated underpotential oxidation of metal electrodes, a Cu electrode for example, allows for the simultaneous formation of composite sulphide/phosphide and oxide nanoparticles. Zeng *et al.* studied the HER performance of a sponge composite of Cu$_x$S and Cu$_x$O nanoparticles that were grown by sulfide-mediated underpotential oxidations of the Cu electrode.[190] It was observed that the Cu$_x$S and Cu$_x$O nanoparticles grew not only at the working electrode but also at the counter electrode doubling the HER activity. The spongy copper composite nanoparticles Cu$_x$S and Cu$_x$O exhibited promising catalytic activity towards the electrochemical production of hydrogen, in which the onset potential, defined at 1.0 mA cm^{-2}, was found to be around – 90 mV for the Cu$_x$S coated electrodes and around –

100 mV for Cu$_x$O coated electrodes (Fig. 18b), with a low Tafel slope of 100 mV dec^{-1}. This work demonstrated the facilitated charge transfer at the Cu$_x$S/Cu$_x$O coating on the copper substrate and paved the way for modified sulphide and phosphide structures of various transition metal oxides as electrocatalysts. Similarly, 3D MoP sponge was reported as a cheap HER electrocatalyst that achieved an excellent catalytic activity of 10 and 20 mA cm^{-2} at an overpotential of 105 and 155 mV, respectively (Fig. 18c), and a slope on the Tafel plot of 126 mV dec^{-1}.[191] It also reached a faradaic efficiency of nearly 100% and a high exchange current density of 3.052 mA cm^{-2}. Moreover, the 3D MoP electrode revealed high tolerance and durability both under acidic and basic conditions, maintaining 96 and 93% of initial catalytic activity even after 60 000 s. 3D dendritic, nano-structured sponge electrodes with abundant micrometre-sized pore networks greatly facilitated the mass transport.

Similarly, Ibupoto *et al.* proposed a robust electrocatalyst composed of MoS$_x$ deposited on NiO nanostructures (MoS$_x$@NiO) to exploit the chemical coupling effect between excess sulphide (MoS$_x$) and NiO/NiS sponges.[37] Chemical coupling approaches impart long activity and adaptability over a larger pH range, increase hydrogen adsorption, and significantly boost reaction kinetics in the nanohybrid material. The excess sulphide groups increase the oxidation state of metal cations, eventually increasing the number of surface-active sites on the MoS$_x$@NiO nanostructure. A HER experiment for MoS$_2$@NiO nanosponge in a 1 M KOH electrolyte showed an overpotential of 406 mV to produce 10 mA cm^{-2} current density (Fig. 18d) and a Tafel slope of 43 mV dec^{-1}, which is lowest ever reported for MoS$_2$-based electrocatalysts. Metallic alloy nanosponges have
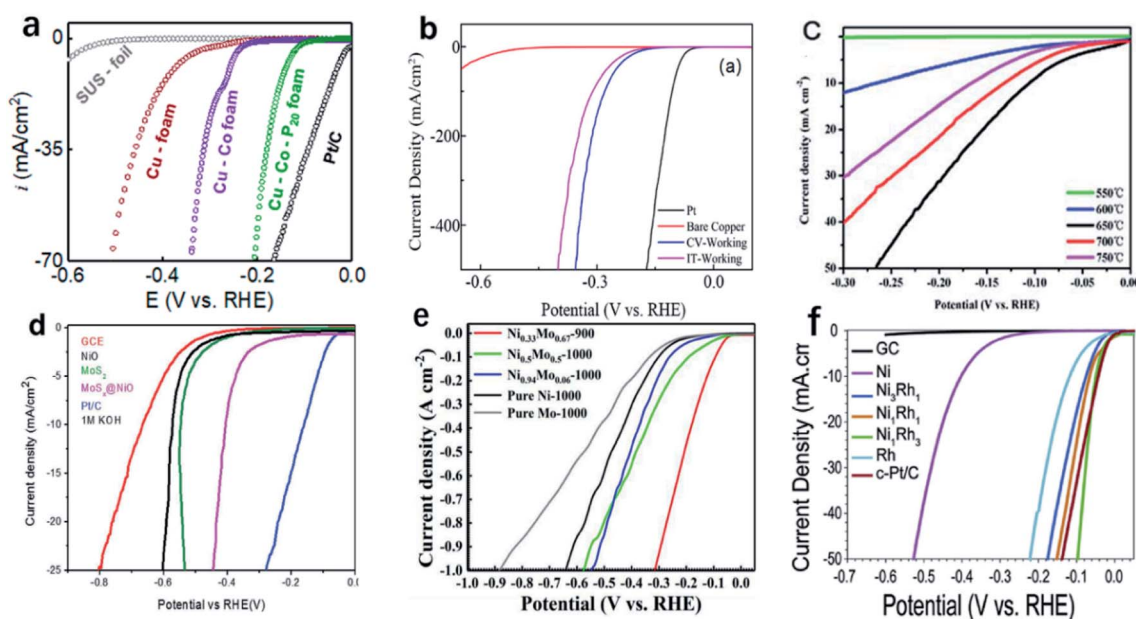
Fig. 18 Linear sweep voltammetry (LSV) HER curves. (a) Cu, Cu–Co and Cu–Co–P$_{20}$ foams. Reproduced with permission.[189] Copyright 2019, American Chemical Society. (b) Modified sponge Cu$_x$S electrodes. Reproduced with permission. Copyright 2019, Wiley-VCH. (c) 3D MoP nanosponge. Reproduced with permission.[191] Copyright 2016, Royal Society of Chemistry. (d) MoS$_x$@NiO composite. Reproduced with permission. Copyright 2019, Wiley-VCH. (e) Pure Ni-1000, pure Mo-1000, Ni$_{0.94}$Mo$_{0.06-1000}$, Ni$_{0.5}$Mo$_{0.5-1000}$ and Ni$_{0.33}$Mo$_{0.67-900}$. Reproduced with permission.[192] Copyright 2020, American Chemical Society. (f) NiRh alloy nanosponges. Reproduced with permission.[197] Copyright 2019, Elsevier.

been extensively explored due to their low cost, high activity, and durability in the HER. In comparison to transition metal sulphide/phosphide nanosponges, metallic alloy nanosponges exhibited better stability, long life, attractive overpotential, and Tafel slope. A metallic alloy nanosponge of NiMo solid solution exhibited a low overpotential and Tafel slope of 37 mV at 10 mA cm^{-2} and 39.2 mV dec^{-1}, respectively (Fig. 18e). Shang et al. attributed such excellent HER activity to the polycrystalline NiMo oxyhydroxide layer formed on the surface of the electrode after aging.[192] The electrode was durable for over 300 h at 2 A cm^{-2} without compromising the electrocatalytic activity, which was attributed to the high conductivity synergistic effect between the Ni and Mo species and 3D-interconnected structure of the nanosponge. Nguyen et al. reported a NiRh alloy nanosponge electrocatalyst, which exhibited an overpotential of 48 mV at a current density of 10 mA cm^{-2} (Fig. 18f) and superior stability up to 2000 cycles.[192] Moreover, the combination of the Ni_1Rh_3 cathode and commercial RuO_2 anode displayed remarkable performance with a potential of 1.52 V at a current density of 10 mA cm^{-2} and very stable operation for over 100 000 s in a 1.0 M KOH electrolyte. This better performance by metallic alloy nanosponges over transition metal sulphide/phosphide nanosponges can be attributed to the enhanced charge transfer between the metal atoms with d electrons.

4.4 OER and ORR

Transition metal chalcogenide nanosponges provide enhanced adsorption and superior charge transfer kinetics and catalytic durability towards electrochemical water splitting. The reason for their superior activity can be attributed to their larger extent of porosity that gives rise to an increased number of active sites. Moreover, a larger number of active sites can be obtained by simply changing the ratio of the metal cation or anion precursors. For example, the Ni_2Fe_1–Mo catalyst showed significantly enhanced activities towards the HER compared with Ni_2Fe_1, by lowering the overpotential of 10 mA cm^{-2} to a scale of 84 mV (Fig. 19a).[193] Nanoporous-$(Ni_{0.67}Fe_{0.33})_4P_5$, a bifunctional nanoporous metal phosphide electrocatalyst, exhibited excellent catalytic performance with overpotentials of 245 mV and 120 mV (Fig. 19b) at a current density of 10 mA cm^{-2} for the OER and HER in 1 M KOH, respectively.[194] The catalytic performance of the nanoporous material was attributed to the similar bi-continuous morphology, disordered atomic arrangement, and phosphates, which acted as charge carriers. However, the study also reported the formation of $Ni_xFe_{1-x}OOH$ during the water-splitting reaction, which could be the actual active species for enhanced HER performance. In an another study, N-doped sponge Ni micro/nanofibers exhibited a larger number of active sites with a faster ion/electron transfer path.[195] The study identified the formation of γ-NiOOH as the active site that accelerated the water oxidation process. Moreover, reduced Ni atoms also serve as an active site for adsorptive bonding on the surface of sponge Ni 3D porous electrocatalysts. The electrocatalysts showed better charge transport as suggested by the smaller Tafel slope. This doping approach can be further adopted for improving the stability and electrochemical
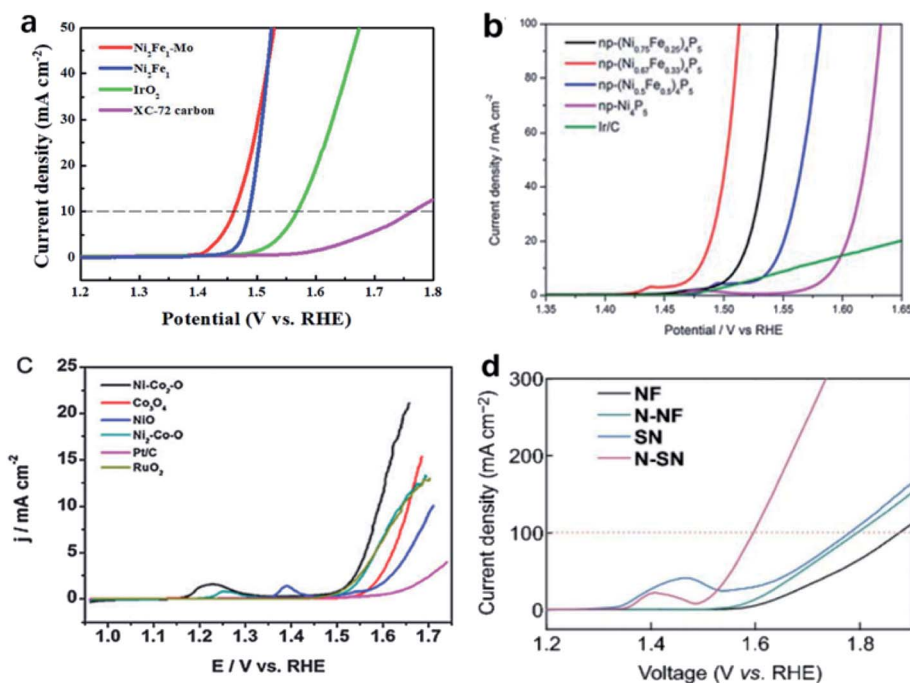
Fig. 19 Linear sweep voltammetry (LSV) OER & ORR curves. (a) Hierarchically porous Mo-doped Ni–Fe. Reproduced with permission.[193] Copyright 2018, Royal Society of Chemistry. (b) Nanoporous np-$(Ni_{0.67}Fe_{0.3})_4P_5$ phosphide catalyst. Reproduced with permission.[194] Copyright 2018, Royal Society of Chemistry. (c) Nickel cobalt oxide hollow nanosponges, Co_3O_4 nanoparticles, and commercial Pt/C. Reproduced with permission.[36] Copyright 2015, Royal Society of Chemistry. (d) Nitrogen-doped sponge Ni fibers NF, N–NF, SN, and N–SN. Reproduced with permission.[195] Copyright 2019, Springer.

This journal is © The Royal Society of Chemistry 2022

J. Mater. Chem. A, 2022, **10**, 14221–14246 | **14239**

efficiency of nanosponge water electrocatalysts. Recently, metal oxides or hydroxides were also reported to produce a large number of active sites, rapid ion/electron transport, and lower electrical resistance and synergistically enhanced catalytic activity due to their intermetallic d-electron stability.[196] The Kirkendall effect, an interface modification process which is used to obtain hollow nanostructures by creating diffusivity differences between the interfaces, was also demonstrated in nickel cobalt oxide nanostructure electrocatalysts.[36] NiCo-hollow nanostructures (HNSs) showed OER (Fig. 19d) activity with the onset potential being as low as 1.5 V, at a small over-potential of 0.362 V. However, without any suitable electrode support material, the anodic current decreased to some extent after 500 cycles, which can be attributed to the instability of the material phase. The efficiency can be further improved by nitrate/phosphate enrichment or by hydrophilic functionalization which could provide an active site for the adsorption of OH ions and hence endowing the electrocatalyst with an excellent OER activity for a longer time.

5. Summary and outlook

Emerging nanosponge materials have been successfully applied in energy storage and conversion applications. The presence of pores in nanosponge materials greatly enhances their electrochemical performances. This review highlights the recent advances in nanosponge materials, particularly noble and non-noble oxides, hydroxides, sulphides and phosphides, primarily emphasising design strategies pertinent to energy storage and conversion utilization, which is summarized in Table 1. Nanosponge materials that belong to the class of porous electrodes are divided into three major categories, namely, monometallic, bimetallic and multimetallic nanosponges. A number of monometallic nanosponges, including and but not limited to Au, Ag, Pt, Pd and Cu, have been fabricated by a template-free or sacrificial template-assisted method. Among them, Au mono-metallic nanosponges have been extensively studied so far, while Pd based sponges have drawn significant research interest owing to the highest catalytic activity, low cost, and stability toward the oxidation reaction. As compared to mono-metallic nanosponges, bimetallic and multimetallic nanosponges show superior electrochemical catalytic properties. Further compositional variety should be pursued to expand the application horizon and to enhance material properties to specific application purposes.

Four major synthetic approaches, namely, dealloying, reduction-based, thermally derived, and electrodeposition, are discussed systematically. The dealloying method involves the etching of a highly active material to effectively fabricate nanosponge structures with good control over pore size distribution. Compared to electrochemical dealloying, chemical dealloying is more preferred mainly due to its operational simplicity. However, the latter process demands highly corrosive acids such as HNO_3 and H_2SO_4 which require careful handling. A template-assisted process is another versatile technique explored for the synthesis of metal and metal oxide nanosponges, where the properties of replicated nanostructures are determined mainly by the structure and features of the templates employed. However, surfactant templates are undesirable for catalytic applications, because additional post-synthesis treatment is required for template removal. In addition, partially filled pores can cause defects and discontinuities, reducing the electrode's performance. Also, the stability of soft templates is poor and requires a strong interaction between the precursors for the synthesis of uniform structures. For these reasons, template-free reduction methods that provide precise control and eliminate the difficulty of removing templates are highly desirable. Kinetically controlled reduction reactions of sodium borohydride are one of such methods explored for bimetallic and trimetallic nanosponges. Nevertheless, their rapid synthesis mechanism has not been fully deciphered. Nanosponges having low-melting temperature and high vapour pressure can be fabricated by thermal decomposition of metal precursors. This method offers a facile approach to prepare nanosponges with a desired composition and morphology. The synthesis process involves heating of precursor solution and the substrate (sponge-like/foam) inside a sealed Teflon autoclave yielding alloy nanosponges. Despite numerous benefits, this approach is limited by the high cost of the autoclave and difficulty in process monitoring. The electrodeposition process benefits from both materials synthesis and electrochemistry that enables atomic scale control to deposit various nanosponge materials precisely. In recent years, hydrogen bubble generation during electrodeposition has been utilized to facilitate the formation of sponge-like porous structures. This 3D porous structure offers a large surface area and active sites and promotes electrolyte–electrode interaction. Furthermore, it also helps the escape of H_2 gas during water splitting. However, the disposal of wastes evolved during the electrodeposition process can severely pollute the environment and raw materials used are expensive. Although significant progress has been made in the synthesis of various nanosponges, there are still limitations in developing novel metallic nanosponges. Since the electrochemical properties of nanosponges are primarily influenced by the pore size, surface area, structural stability, and composition, it is essential to develop an economical and reliable method that provides precise control over these parameters and is also eco-friendly. Moreover, the considerably more sophisticated production procedures and associated costs are among the major impediments to the commercialization of nanosponge materials in the current energy market sector. However, these challenges can be subjugated with advancements in process engineering and improvement in system performance such as hydrothermal, solvothermal, self-assembly, and template-based that operate on commercial materials at the industrial level.

Substantial progress has been made for adopting nanosponge electrodes for the applications of energy storage and energy conversion. Their unique sponge morphology promotes shorter diffusion paths for rapid charge transfer, decreasing the internal resistance to enhance the rate capabilities. Nevertheless, there are a few disadvantages to be resolved before their deployment into practical applications. Firstly, the large surface area combined with defects can lead to unwanted side reactions especially in batteries having liquid electrolytes. This might

14240 | *J. Mater. Chem. A*, 2022, **10**, 14221–14246

This journal is © The Royal Society of Chemistry 2022

Table 1 Summary of nanosponge materials in electrochemical and energy conversion applications

Battery

Nanosponge	Application	Initial charge capacity (mA h g^{-1}@A g^{-1})	Cycling performance (capacitance retention/cycles@A g^{-1})	Electrolyte	Ref.
CuO ribbon clusters	LiB anode	638@0.2C	81%/50@0.2C	1 M $LiPF_6$ in EC–DEC at a 1 : 1 volume ratio	162
Au	LiB anode	~500@15 µA cm^{-2} (discharge)	80/30@15 µA cm^{-2}	1 M $LiPF_6$ in EC–DMC at a 1 : 1 volume ratio	160
Nanoporous FTO	LiB anode	1900@0.1C	470/50@0.1C	1.2 M $LiPF_6$ in EC–EMC at a 3 : 7 weight ratio	161
CuO	LiB anode	—	—	1 M $LiPF_6$ in EC–DEC at a 1 : 1 volume ratio	135
Mn_3O_4	LiB anode	869@0.25C	800/40@0.25C	1 M $LiPF_6$ in EC–DEC at a 1 : 1 volume ratio	163
$Ni_{1.8}Fe_{1.2}O_4$ nanocubes	LiB anode	846.8@2	910/75@2	1 M $LiPF_6$ in DEC–DC–EC at a 1 : 1 : 1 volume ratio	198
V_2O_5-SLMNS	LiB cathode	232@1	87%/50@1	1 M $LiPF_6$ in EC–DEC at a 1 : 1 volume ratio	159
$LiMn_2O_4$ thin-films	LiB cathode	—	—	1 M $LiPF_6$ in EC–DEC at a 1 : 1 volume ratio	147
SEI@Li/SN	LSB anode	784.9@1C	99.82%/200@1C	1 M $LiPF_6$ in EC–DEC at a 1 : 1 volume ratio	172
Li_7B_6	LSB anode	1072@1	694/100@1	0.4 M LiTFSI in DOL–DME at a 1 : 1 volume ratio with 0.4 M $LiNO_3$ as the additive	174
ε-MnO_2/Ni	LiO_2 cathode	6300@0.5	>1000/120@0.5	1 M LiTFSI in TEGDME	148
V_2O_5	NiB cathode	216@0.02	73%/100@0.1	1 M $NaClO_4$ in PC with 2% FEC as the additive	122
$Na_3V_2(PO_4)_3$	NiB cathode	101.77@50C	89.28/700@30C	1 M $NaClO_4$ in PC with 2% FEC as the additive	180
Zn	Ag–Zn cells	~780@55	—	6 M KOH	184
Zn	Zn–air cells	743@55	—	6 M KOH/poly(acrylic acid)	183

Supercapacitor

Nanosponge	Specific capacity	Loading (mg cm^{-2})	Cycling performance	Electrolyte	Ref.
$NiCo_2S_4$	11.97 F cm^{-2}@15 mA cm^{-2}	18.7	80.1%/5000@40 mA cm^{-2}	2 M KOH	185
$Ni(OH)_2$–NiF_2	1680 F g^{-1}@100 A g^{-1}	0.15	>1200 F g^{-1}/2000@100 A g^{-1}	1 wt% NH_4F + 80 wt% H_3PO_4	186
VO_2/TiO_2	715.8 F g^{-1}@5 A g^{-1}	0.1533	84.3%/1000@10 A g^{-1}	8 M LiCl	154
Bi_2O_3	536 F g^{-1}@2 A g^{-1}	~4.42 mg	85%/5000@2 A g^{-1}	6 M KOH	188
Mn_3O_4	274 F g^{-1}@0.5 A g^{-1}	~2 mg	98.9%/5000@2 A g^{-1}	1 M Na_2SO_4	187

HER

Nanosponge	Overpotential at 10 mA cm^2 (mV)	Tafel slope (mV dec^{-1})	Loading (mg cm^{-2})	Electrolyte	Ref.
Ni_2Fe_1–Mo	147	128	0.25	1 M KOH	193
Cu–Co–P_{20}	138	48	0.76	1 M KOH	189
MoP	105	126	0.35	0.5 M H_2SO_4	191
MoS_x@NiO	406	43	—	1 M KOH	37
NiAu–P	88	37	~0.169	0.5 M H_2SO_4	67
$Ni_{0.33}Mo_{0.67}$–900	37	39.2	—	1 M KOH	192
Ni_1Rh_3	48	~31	~0.169	0.5 M H_2SO_4	197
Ni_1Rh_3	107	~75	~0.169	1 M KOH	197
$Pt_{53}Ru_{39}Ni_8$	37	34	—	0.5 M H_2SO_4	70
$Pt_{53}Ru_{39}Ni_8$	40	46	—	0.5 M KOH	70

This journal is © The Royal Society of Chemistry 2022

J. Mater. Chem. A, 2022, **10**, 14221–14246 | **14241**

Table 1 (*Contd.*)

OER

Nanosponge	Overpotential at 10 mA cm^{-2} (mV)	Tafel slope (mV dec^{-1})	Loading (mg cm^{-2})	Electrolyte	Ref.
Ni$_2$Fe$_1$–Mo	231	39	0.20	1 M KOH	193
N doped sponge Ni	365 (100 mA cm^{-2})	33	—	1 M KOH	195
Ni–Co$_2$–O	362	64.4	0.20	0.1 M KOH	36
Ni$_1$Co$_2$	1692	87.3	10	0.1 M KOH	32
NiCo-200	420	157	0.71	1 M KOH	138

lead to consumption of the electrolyte and ineffective utilization of the active material, resulting in poor battery performance. Porous nanosponge electrode materials do not consistently outperform traditional materials in terms of capacity at slow charge and discharge rates. Furthermore, fine-tuning the material design on the nanoscale might bring about additional costs, which is not desirable. Not leveraging the entire porous structure and low packing density also are the drawbacks in volumetric energy and power density, which can only increase the space required to store a certain amount of energy. This limitation can be resolved by adequately enabling the porous structure of nanosponges' materials with higher bulk energy density. Moreover, a nanosponge has interconnected channels that are not stable at high temperatures resulting in a poor catalytic performance at a wide range of temperatures. Our understanding of the intricate mechanisms of electrochemistry and reaction kinetics at nanosponge-based electrodes is only at the infancy, which requires a great deal of theoretical and operando experiments specifically suited for nanosponge structures. New findings and thoughts are required to accrue the benefits of nanosponge materials and resolve their challenges, providing intriguing chances for those entering this field. Extensive future research and direction must be emphasised towards (1) the design and scalable synthesis process of novel multimetallic nanosponge materials by considering performance and cost, (2) developing advanced fabrication techniques for surface engineering nanosponge materials to obtain a preferred crystal facet, abundant active sites, vacancies, and homogeneous doping throughout the material, (3) precise tailoring of pore channels, pore size on different length scales, and crystallinity to minimize the possibility of side reactions, maximize mass transport, and improve thermal stability, respectively, (4) thorough understanding of mass transport dynamics and kinetics occurring within nanostructured materials that can bridge the gap between nanoscale effects and overall system performance, and (5) development of Li alternative nanosponge compositions that can give a commercially viable option for non-LiBs because current LiB electrode materials may become scarce in the near future. We believe that our timely review provides critical insights into the current research of nanosponge materials for energy storage and conversion systems and opens pathways for the development of next-generation electrical energy storage and generation devices.

Conflicts of interest

The authors declare that there are no competing interests.

Acknowledgements

Notes and references

1 B. Dunn, H. Kamath and J.-M. Tarascon, *Science*, 2011, **334**, 928–935.

2 S. Chu and A. Majumdar, *Nature*, 2012, **488**, 294–303.

3 Z. Yang, J. Zhang, M. C. W. Kintner-Meyer, X. Lu, D. Choi, J. P. Lemmon and J. Liu, *Chem. Rev.*, 2011, **111**, 3577–3613.

4 R. Seshadri, K. Persson, P. V. Kamat and Y. Wu, *Chem. Mater.*, 2015, **27**, 4505–4506.

5 G. M. Tomboc, B. Tesfaye Gadisa, M. Jun, N. K. Chaudhari, H. Kim and K. Lee, *Chem.–Asian J.*, 2020, **15**, 1628–1647.

6 A. M. Abdalla, S. Hossain, A. T. Azad, P. M. I. Petra, F. Begum, S. G. Eriksson and A. K. Azad, *Renewable Sustainable Energy Rev.*, 2018, **82**, 353–368.

7 H. Jin, B. Ruqia, Y. Park, H. J. Kim, H. Oh, S. Choi and K. Lee, *Adv. Energy Mater.*, 2021, **11**, 2003188.

8 G. Centi and S. Perathoner, *Eur. J. Inorg. Chem.*, 2009, **2009**, 3851–3878.

9 Q. Zhang, E. Uchaker, S. L. Candelaria and G. Cao, *Chem. Soc. Rev.*, 2013, **42**, 3127.

10 Y. Liu, G. Zhou, K. Liu and Y. Cui, *Acc. Chem. Res.*, 2017, **50**, 2895–2905.

14242 | *J. Mater. Chem. A*, 2022, **10**, 14221–14246

This journal is © The Royal Society of Chemistry 2022

11 N. K. Chaudhari, H. Jin, B. Kim and K. Lee, *Nanoscale*, 2017, **9**, 12231–12247.

12 A. S. Aricò, P. Bruce, B. Scrosati, J.-M. Tarascon and W. van Schalkwijk, *Nat. Mater.*, 2005, **4**, 366–377.

13 H. Bin Wu, G. Zhang, L. Yu and X. W. (David) Lou, *Nanoscale Horiz.*, 2016, **1**, 27–40.

14 N. R. Hemanth and B. Kandasubramanian, *Chem. Eng. J.*, 2019, 123678.

15 M. Chhowalla, H. S. Shin, G. Eda, L.-J. Li, K. P. Loh and H. Zhang, *Nat. Chem.*, 2013, **5**, 263–275.

16 D. S. Su and R. Schlögl, *ChemSusChem*, 2010, **3**, 136–168.

17 J. Liu, Z. Bao, Y. Cui, E. J. Dufek, J. B. Goodenough, P. Khalifah, Q. Li, B. Y. Liaw, P. Liu, A. Manthiram, Y. S. Meng, V. R. Subramanian, M. F. Toney, V. V. Viswanathan, M. S. Whittingham, J. Xiao, W. Xu, J. Yang, X.-Q. Yang and J.-G. Zhang, *Nat. Energy*, 2019, **4**, 180–186.

18 Y. Shi, L. Peng, Y. Ding, Y. Zhao and G. Yu, *Chem. Soc. Rev.*, 2015, **44**, 6684–6696.

19 Y. Yang, L. Zhao, K. Shen, Y. Liu, X. Zhao, Y. Wu, Y. Wang and F. Ran, *J. Power Sources*, 2016, **333**, 61–71.

20 Z.-S. Wu, W. Ren, L. Wen, L. Gao, J. Zhao, Z. Chen, G. Zhou, F. Li and H.-M. Cheng, *ACS Nano*, 2010, **4**, 3187–3194.

21 W. Wang, F. Lv, B. Lei, S. Wan, M. Luo and S. Guo, *Adv. Mater.*, 2016, **28**, 10117–10141.

22 N. K. Chaudhari, H. Jin, B. Kim, D. San Baek, S. H. Joo and K. Lee, *J. Mater. Chem. A*, 2017, **5**, 24564–24579.

23 E. Pomerantseva and Y. Gogotsi, *Nat. Energy*, 2017, **2**, 17089.

24 B. L. Ellis, P. Knauth and T. Djenizian, *Adv. Mater.*, 2014, **26**, 3368–3397.

25 H. Sun, L. Mei, J. Liang, Z. Zhao, C. Lee, H. Fei, M. Ding, J. Lau, M. Li, C. Wang, X. Xu, G. Hao, B. Papandrea, I. Shakir, B. Dunn, Y. Huang and X. Duan, *Science*, 2017, **356**, 599–604.

26 X.-Y. Yang, L.-H. Chen, Y. Li, J. C. Rooke, C. Sanchez and B.-L. Su, *Chem. Soc. Rev.*, 2017, **46**, 481–558.

27 E. Pomerantseva, F. Bonaccorso, X. Feng, Y. Cui and Y. Gogotsi, *Science*, 2019, **366**, eaan8285.

28 N. R. Hemanth, T. Kim, B. Kim, A. H. Jadhav, K. Lee and N. K. Chaudhari, *Mater. Chem. Front.*, 2021, **5**, 3298–3321.

29 H. Zhao and Y. Lei, *Adv. Energy Mater.*, 2020, **10**, 2001460.

30 P. Balaya, *Energy Environ. Sci.*, 2008, **1**, 645.

31 N. R. Hemanth and B. Kandasubramanian, *Chem. Eng. J.*, 2020, **392**, 123678.

32 T. V. Vineesh, S. Mubarak, M. G. Hahm, V. Prabu, S. Alwarappan and T. N. Narayanan, *Sci. Rep.*, 2016, **6**, 1–9.

33 N. A. Nguyen, Y. Ali, V. T. Nguyen, O. Omelianovych, L. L. Larina and H. S. Choi, *J. Alloys Compd.*, 2020, **849**, 156651.

34 T. Zhang, F. Zhou, L. Hang, Y. Sun, D. Liu, H. Li, G. Liu, X. Lyu, C. Li, W. Cai and Y. Li, *J. Mater. Chem. C*, 2017, **5**, 11039–11045.

35 S. Surendran, S. Shanmugapriya, S. Shanmugam, L. Vasylechko and R. Kalai Selvan, *ACS Appl. Energy Mater.*, 2018, **1**, 78–92.

36 C. Zhu, D. Wen, S. Leubner, M. Oschatz, W. Liu, M. Holzschuh, F. Simon, S. Kaskel and A. Eychmüller, *Chem. Commun.*, 2015, **51**, 7851–7854.

37 Z. H. Ibupoto, A. Tahira, P. Y. Tang, X. Liu, J. R. Morante, M. Fahlman, J. Arbiol, M. Vagin and A. Vomiero, *Adv. Funct. Mater.*, 2019, **29**, 1–10.

38 M. Tebyetekerwa, X. Wang, Y. Wu, S. Yang, M. Zhu and S. Ramakrishna, *J. Mater. Chem. A*, 2017, **5**, 21114–21121.

39 Z. Li and L. Yin, *Nanoscale*, 2015, **7**, 9597–9606.

40 J. C. Li, P. X. Hou, S. Y. Zhao, C. Liu, D. M. Tang, M. Cheng, F. Zhang and H. M. Cheng, *Energy Environ. Sci.*, 2016, **9**, 3079–3084.

41 Y.-G. Guo, J.-S. Hu and L.-J. Wan, *Adv. Mater.*, 2008, **20**, 2878–2887.

42 R. Yadav, A. Subhash, N. Chemmenchery and B. Kandasubramanian, *Ind. Eng. Chem. Res.*, 2018, **57**, 9333–9350.

43 H. Zhou, M. Liu, Y. Li, C. Liu, H. Gao, Z. Cao, D. Zhang, X. Jin, Q. Chen, Y. Liu and J. Yang, *J. Electrochem. Soc.*, 2018, **165**, A3100–A3107.

44 S. Bose, T. Kuila, A. K. Mishra, R. Rajasekar, N. H. Kim and J. H. Lee, *J. Mater. Chem.*, 2012, **22**, 767–784.

45 L. Li, S. Mahapatra, D. Liu, Z. Lu and N. Jiang, *ACS Nano*, 2021, **15**, 3578–3585.

46 Y. Li, Z.-Y. Fu and B.-L. Su, *Adv. Funct. Mater.*, 2012, **22**, 4634–4667.

47 Z. Su and T. Chen, *Small*, 2021, **17**, 2005354.

48 A. Vu, Y. Qian and A. Stein, *Adv. Energy Mater.*, 2012, **2**, 1056–1085.

49 D. Walsh, L. Arcelli, T. Ikoma, J. Tanaka and S. Mann, *Nat. Mater.*, 2003, **2**, 386–390.

50 M. Dong, Y. X. Zhang, H. F. Song, X. Qiu, X. D. Hao, C. P. Liu, Y. Yuan, X. L. Li and J. M. Huang, *Phys. E*, 2012, **45**, 103–108.

51 H. Ataee-Esfahani, Y. Nemoto, L. Wang and Y. Yamauchi, *Chem. Commun.*, 2011, **47**, 3885.

52 M. T. Islam, J. Rosales, R. Saenz-Arana, R. Arrieta, H. Kim, K. A. Sultana, Y. Lin, D. Villagran and J. C. Noveron, *New J. Chem.*, 2019, **43**, 10045–10055.

53 K. S. Krishna, C. S. S. Sandeep, R. Philip and M. Eswaramoorthy, *ACS Nano*, 2010, **4**, 2681–2688.

54 S. Ghosh and B. R. Jagirdar, *ChemistrySelect*, 2018, **3**, 7184–7194.

55 S. Tang, S. Vongehr, Y. Wang, J. Cui, X. Wang and X. Meng, *J. Mater. Chem. A*, 2014, **2**, 3648–3660.

56 F. Yu, W. Zhou, R. M. Bellabarba and R. P. Tooze, *Nanoscale*, 2014, **6**, 1093–1098.

57 Y. Yan, A. I. Radu, W. Rao, H. Wang, G. Chen, K. Weber, D. Wang, D. Cialla-May, J. Popp and P. Schaaf, *Chem. Mater.*, 2016, **28**, 7673–7682.

58 T. Zhang, F. Zhou, L. Hang, Y. Sun, D. Liu, H. Li, G. Liu, X. Lyu, C. Li, W. Cai and Y. Li, *J. Mater. Chem. C*, 2017, **5**, 11039–11045.

59 J. Wang, F. Chen, Y. Jin and Y. Lei, *ACS Appl. Mater. Interfaces*, 2018, **10**, 6276–6287.

60 N. K. Chaudhari, Y. Hong, B. Kim, S.-I. Choi and K. Lee, *J. Mater. Chem. A*, 2019, **7**, 17183–17203.

This journal is © The Royal Society of Chemistry 2022

J. Mater. Chem. A, 2022, **10**, 14221–14246 | **14243**

61 N. K. Chaudhari, J. Joo, B. Kim, B. Ruqia, S.-I. Choi and K. Lee, *Nanoscale*, 2018, **10**, 20073–20088.

62 Z. Zhu, Y. Zhai and S. Dong, *ACS Appl. Mater. Interfaces*, 2014, **6**, 16721–16726.

63 C. Zhu, S. Guo and S. Dong, *Chem.–Eur. J.*, 2013, **19**, 1104–1111.

64 W. Luo, H. Zhou, C. Fu, Z. Huang, N. Gao and Y. Kuang, *Mater. Lett.*, 2016, **173**, 43–46.

65 Y. Yu, Z. Huang, D. Deng, Y. Ju, L. Ren, M. Xiang, L. Li and H. Li, *Chem. Eng. J.*, 2017, **325**, 279–288.

66 Y. S. Park, W. S. Choi, M. J. Jang, J. H. Lee, S. Park, H. Jin, M. H. Seo, K. H. Lee, Y. Yin, Y. Kim, J. Yang and S. M. Choi, *ACS Sustainable Chem. Eng.*, 2019, **7**, 10734–10741.

67 N. A. Nguyen, T. T. T. Nguyen, V. T. Nguyen, Y. Ali, E. Sim and H. S. Choi, *Catal. Today*, 2019, **337**, 90–96.

68 C.-L. Lee, Y.-C. Huang, L.-C. Kuo, J.-C. Oung and F.-C. Wu, *Nanotechnology*, 2006, **17**, 2390–2395.

69 S. Li, J. Lai, R. Luque and G. Xu, *Energy Environ. Sci.*, 2016, **9**, 3097–3102.

70 Y. C. Shi, T. Yuan, J. J. Feng, J. Yuan and A. J. Wang, *J. Colloid Interface Sci.*, 2017, **505**, 14–22.

71 J. Erlebacher, M. J. Aziz, A. Karma, N. Dimitrov and K. Sieradzki, *Nature*, 2001, **410**, 450–453.

72 C. Zhu, D. Du, A. Eychmüller and Y. Lin, *Chem. Rev.*, 2015, **115**, 8896–8943.

73 A.-A. El Mel, F. Boukli-Hacene, L. Molina-Luna, N. Bouts, A. Chauvin, D. Thiry, E. Gautron, N. Gautier and P.-Y. Tessier, *ACS Appl. Mater. Interfaces*, 2015, **7**, 2310–2321.

74 T. Fujita, P. Guan, K. McKenna, X. Lang, A. Hirata, L. Zhang, T. Tokunaga, S. Arai, Y. Yamamoto, N. Tanaka, Y. Ishikawa, N. Asao, Y. Yamamoto, J. Erlebacher and M. Chen, *Nat. Mater.*, 2012, **11**, 775–780.

75 V. Zielasek, B. Jürgens, C. Schulz, J. Biener, M. M. Biener, A. V. Hamza and M. Bäumer, *Angew. Chem., Int. Ed.*, 2006, **45**, 8241–8244.

76 T. Fujita, L.-H. Qian, K. Inoke, J. Erlebacher and M.-W. Chen, *Appl. Phys. Lett.*, 2008, **92**, 251902.

77 Z.-H. Lin, Z.-Y. Shih, H.-Y. Tsai and H.-T. Chang, *Green Chem.*, 2011, **13**, 1029.

78 T. Zheng, G. G. Li, F. Zhou, R. Wu, J.-J. Zhu and H. Wang, *Adv. Mater.*, 2016, **28**, 8218–8226.

79 J.-M. Yi, D. Wang, F. Schwarz, J. Zhong, A. Chimeh, A. Korte, J. Zhan, P. Schaaf, E. Runge and C. Lienau, *ACS Photonics*, 2019, **6**, 2779–2787.

80 G. G. Li, Y. Lin and H. Wang, *Nano Lett.*, 2016, **16**, 7248–7253.

81 H. Xu, S. Pang, Y. Jin and T. Zhang, *Nano Res.*, 2016, **9**, 2467–2477.

82 B. Kumar Barman and K. Kar Nanda, *Dalton Trans.*, 2015, **44**, 4215–4222.

83 G. G. Li, E. Villarreal, Q. Zhang, T. Zheng, J.-J. Zhu and H. Wang, *ACS Appl. Mater. Interfaces*, 2016, **8**, 23920–23931.

84 D. Wang and P. Schaaf, *Adv. Phys.: X*, 2018, **3**, 1456361.

85 S. Cattarin, D. Kramer, A. Lui and M. Musiani, *Fuel Cells*, 2009, **9**, 209–214.

86 Y. Sun and T. J. Balk, *Scr. Mater.*, 2008, **58**, 727–730.

87 Z. Yi, J. Luo, X. Tan, Y. Yi, W. Yao, X. Kang, X. Ye, W. Zhu, T. Duan, Y. Yi and Y. Tang, *Sci. Rep.*, 2015, **5**, 16137.

88 S. Tominaka, T. Hayashi, Y. Nakamura and T. Osaka, *J. Mater. Chem.*, 2010, **20**, 7175.

89 F. Chen, J.-H. Li, Y.-C. Chi, Z.-H. Dan and F.-X. Qin, *J. Nanosci. Nanotechnol.*, 2020, **20**, 7333–7341.

90 F. Cheng, Z. Tao, J. Liang and J. Chen, *Chem. Mater.*, 2008, **20**, 667–681.

91 K. Lee, Y.-H. Kim, S. B. Han, H. Kang, S. Park, W. S. Seo, J. T. Park, B. Kim and S. Chang, *J. Am. Chem. Soc.*, 2003, **125**, 6844–6845.

92 H. Kang, Y. Jun, J.-I. Park, K.-B. Lee and J. Cheon, *Chem. Mater.*, 2000, **12**, 3530–3532.

93 H. Wang, H. Y. Jeong, M. Imura, L. Wang, L. Radhakrishnan, N. Fujita, T. Castle, O. Terasaki and Y. Yamauchi, *J. Am. Chem. Soc.*, 2011, **133**, 14526–14529.

94 H. J. Shin, C. H. Ko and R. Ryoo, *J. Mater. Chem.*, 2001, **11**, 260–261.

95 M. Clay, Q. Cui, Y. Sha, J. Chen, A. J. Rondinone, Z. Wu, J. Chen and Z. Gu, *Mater. Lett.*, 2012, **88**, 143–147.

96 Y.-H. Chang, C. Liu and S.-P. Feng, *Thin Solid Films*, 2016, **603**, 1–7.

97 Y. Xu and B. Zhang, *Chem. Soc. Rev.*, 2014, **43**, 2439.

98 G. S. Attard, J. M. Corker, C. G. Göltner, S. Henke and R. H. Templer, *Angew. Chem., Int. Ed. Engl.*, 1997, **36**, 1315–1317.

99 G. S. Attard, *Science*, 1997, **278**, 838–840.

100 G. S. Attard, S. A. A. Leclerc, S. Maniguet, A. E. Russell, I. Nandhakumar and P. N. Bartlett, *Chem. Mater.*, 2001, **13**, 1444–1446.

101 F. Bender, R. K. Mankelow, D. B. Hibbert and J. J. Gooding, *Electroanalysis*, 2006, **18**, 1558–1563.

102 R. Campbell, M. G. Bakker, C. Treiner and J. Chevalet, *J. Porous Mater.*, 2004, **11**, 63–69.

103 Y. Yamauchi and K. Kuroda, *Chem.–Asian J.*, 2008, **3**, 664–676.

104 Y. Yamauchi, M. Komatsu, A. Takai, R. Sebata, M. Sawada, T. Momma, M. Fuziwara, T. Osaka and K. Kuroda, *Electrochim. Acta*, 2007, **53**, 604–609.

105 R. R. Poolakkandy and M. M. Menamparambath, *Nanoscale Adv.*, 2020, **2**, 5015–5045.

106 S. Gao, H. Zhang, X. Wang, J. Yang, L. Zhou, C. Peng, D. Sun and M. Li, *Nanotechnology*, 2005, **16**, 2530–2535.

107 D.-H. Yu, X. Yu, C. Wang, X.-C. Liu and Y. Xing, *ACS Appl. Mater. Interfaces*, 2012, **4**, 2781–2787.

108 A. G. M. da Silva, T. S. Rodrigues, S. J. Haigh and P. H. C. Camargo, *Chem. Commun.*, 2017, **53**, 7135–7148.

109 B.-S. Choi, Y. W. Lee, S. W. Kang, J. W. Hong, J. Kim, I. Park and S. W. Han, *ACS Nano*, 2012, **6**, 5659–5667.

110 M. U. D. Sheikh, G. A. Naikoo, M. Thomas, M. Bano and F. Khan, *J. Sol-Gel Sci. Technol.*, 2015, **76**, 572–581.

111 F. Khan and S. Mann, *J. Phys. Chem. C*, 2009, **113**, 19871–19874.

112 S. Kwak, S. Jang, S. Park, J. Kang, T. Y. Kim and I. Nam, *Scr. Mater.*, 2021, **196**, 113769.

14244 | *J. Mater. Chem. A*, 2022, **10**, 14221–14246

This journal is © The Royal Society of Chemistry 2022

113 G. Tong, F. Du, L. Xiang, F. Liu, L. Mao and J. Guan, *Nanoscale*, 2014, **6**, 778–787.

114 W. Shi, S. Song and H. Zhang, *Chem. Soc. Rev.*, 2013, **42**, 5714.

115 G. M. Tomboc, J. Kim, Y. Wang, Y. Son, J. Li, J. Y. Kim and K. Lee, *J. Mater. Chem. A*, 2021, **9**, 4528–4557.

116 Y. X. Zhang and H. C. Zeng, *J. Phys. Chem. C*, 2007, **111**, 6970–6975.

117 Y. X. Gan, A. H. Jayatissa, Z. Yu, X. Chen and M. Li, *J. Nanomater.*, 2020, **2020**, 1–3.

118 X. Wang, H. Huang, G. Li, Y. Liu, J. Huang and D.-P. Yang, *Nanoscale Res. Lett.*, 2014, **9**, 648.

119 F. Shi, D. Xie, Y. Zhong, D. H. Wang, X. H. Xia, C. D. Gu, X. L. Wang and J. P. Tu, *J. Power Sources*, 2016, **328**, 405–412.

120 Y. Lu, J. Liu, X. Liu, S. Huang, T. Wang, X. Wang, C. Gu, J. Tu and S. X. Mao, *CrystEngComm*, 2013, **15**, 7071.

121 Z. Zhang, S. Liu, J. Xiao and S. Wang, *J. Mater. Chem. A*, 2016, **4**, 9691–9699.

122 K. Zhu, C. Zhang, S. Guo, H. Yu, K. Liao, G. Chen, Y. Wei and H. Zhou, *ChemElectroChem*, 2015, **2**, 1660–1664.

123 M. Pang, G. Long, S. Jiang, Y. Ji, W. Han, B. Wang, X. Liu, Y. Xi, D. Wang and F. Xu, *Chem. Eng. J.*, 2015, **280**, 377–384.

124 M. Zhu, X. Zhang, Y. Zhou, C. Zhuo, J. Huang and S. Li, *RSC Adv.*, 2015, **5**, 39270–39277.

125 G. Cheng, J. Xiong, H. Yang, Z. Lu and R. Chen, *Mater. Lett.*, 2012, **77**, 25–28.

126 W. Lu, K. He, G. Zhao, B. Song, J. Zhou, W. Dong and G. Han, *RSC Adv.*, 2019, **9**, 22772–22778.

127 S. Chandrasekaran, L. Yao, L. Deng, C. Bowen, Y. Zhang, S. Chen, Z. Lin, F. Peng and P. Zhang, *Chem. Soc. Rev.*, 2019, **48**, 4178–4280.

128 M. Liu, G. Li and X. Chen, *ACS Appl. Mater. Interfaces*, 2014, **6**, 2604–2610.

129 P. Kulkarni, S. K. Nataraj, R. G. Balakrishna, D. H. Nagaraju and M. V. Reddy, *J. Mater. Chem. A*, 2017, **5**, 22040–22094.

130 F. Chen, H. Wang, S. Ji, V. Linkov and R. Wang, *Mater. Today Energy*, 2019, **11**, 211–217.

131 Y. Du, B. Yu, L. Wei, Y. Wang, X. Zhang and S. Ye, *J. Mater. Sci.*, 2019, **54**, 13283–13297.

132 Y. Wang, Z. Wang, L. Zhao, Q. Fan, X. Zeng, S. Liu, W. K. Pang, Y. He and Z. Guo, *Adv. Mater.*, 2021, **33**, 2008133.

133 X. Fan, X. Qin, L. Jing, Y. Luan and M. Xie, *Mater. Res. Bull.*, 2012, **47**, 3732–3737.

134 N. Kumar, D. Mishra, S. Yeob Kim, T. Na and S. Hun Jin, *Mater. Lett.*, 2020, **279**, 128467.

135 C. S. Choi, Y.-U. Park, H. Kim, N. R. Kim, K. Kang and H. M. Lee, *Electrochim. Acta*, 2012, **70**, 98–104.

136 N. Droushiotis, U. Doraswami, K. Kanawka, G. H. Kelsall and K. Li, *Solid State Ionics*, 2009, **180**, 1091–1099.

137 A. P. Naik, A. V. Salkar, G. D. J. G. Peña, J. V. Sawant, G. Bharath, F. Banat, S. V. Bhosale and P. P. Morajkar, *J. Mater. Sci.*, 2020, **55**, 12232–12248.

138 S. V. Sheen Mers and V. Ganesh, *SN Appl. Sci.*, 2020, **2**, 1149.

139 W. S. dos Santos, L. D. Almeida, A. S. Afonso, M. Rodriguez, J. P. Mesquita, D. S. Monteiro, L. C. A. Oliveira, J. D. Fabris and M. C. Pereira, *Appl. Catal., B*, 2016, **182**, 247–256.

140 S. Saha and S. Das, in *Chemical Solution Synthesis for Materials Design and Thin Film Device Applications*, Elsevier, 2021, pp. 561–583.

141 X. Li and C. Wang, *J. Mater. Chem. A*, 2013, **1**, 165–182.

142 A. Lahiri and F. Endres, *J. Electrochem. Soc.*, 2017, **164**, D597–D612.

143 G.-R. Li, H. Xu, X.-F. Lu, J.-X. Feng, Y.-X. Tong and C.-Y. Su, *Nanoscale*, 2013, **5**, 4056.

144 Z. Yan, H. Liu, Z. Hao, M. Yu, X. Chen and J. Chen, *Chem. Sci.*, 2020, **11**, 10614–10625.

145 D. P. Dubal, S. H. Lee and W. B. Kim, *J. Mater. Sci.*, 2012, **47**, 3817–3821.

146 M. Jin, G. Zhang, F. Yu, W. Li, W. Lu and H. Huang, *Phys. Chem. Chem. Phys.*, 2013, **15**, 1601–1605.

147 J. L. Shui, G. S. Jiang, S. Xie and C. H. Chen, *Electrochim. Acta*, 2004, **49**, 2209–2213.

148 X. Hu, X. Han, Y. Hu, F. Cheng and J. Chen, *Nanoscale*, 2014, **6**, 3522.

149 J. Zhou, B. Zhao, J. Song, B. Chen, J. Bai, Z. Fang, J. Dai, X. Zhu and Y. Sun, *ACS Appl. Energy Mater.*, 2019, **2**, 354–362.

150 Y. Yang, H. Fei, G. Ruan, C. Xiang and J. M. Tour, *Adv. Mater.*, 2014, **26**, 8163–8168.

151 Y. Li, Y.-Y. Song, C. Yang and X.-H. Xia, *Electrochem. Commun.*, 2007, **9**, 981–988.

152 S. Vesztergom, A. Dutta, M. Rahaman, K. Kiran, I. Zelocualtecatl Montiel and P. Broekmann, *ChemCatChem*, 2021, **13**, 1039–1058.

153 W.-S. Choi and H.-C. Shin, *J. Alloys Compd.*, 2017, **692**, 670–675.

154 C. Hu, H. Xu, X. Liu, F. Zou, L. Qie, Y. Huang and X. Hu, *Sci. Rep.*, 2015, **5**, 16012.

155 S. Lang, M. Türk and B. Kraushaar-Czarnetzki, *J. Catal.*, 2012, **286**, 78–87.

156 E. V. Skorb and D. V. Andreeva, *J. Mater. Chem. A*, 2013, **1**, 7547.

157 E. Skorb and D. Shchukin, Controlled Sonochemical Fabrication of Mesoporous Surfaces and Metal Sponges, in *Cavitation*, 2014, pp. 343–379, DOI: **10.1201/b15669-12**.

158 S. Syubaev, S. Gurbatov, E. Modin, D. P. Linklater, S. Juodkazis, E. L. Gurevich and A. Kuchmizhak, *Nanomaterials*, 2020, **10**, 2427.

159 P. Liu, K. Zhu, K. Bian, Y. Xu, F. Zhang, W. Zhang, J. Zhang and W. Huang, *J. Alloys Compd.*, 2018, **765**, 901–906.

160 L. Yuan, H. K. Liu, A. Maaroof, K. Konstantinov, J. Liu and M. Cortie, *J. New Mater. Electrochem. Syst.*, 2007, **10**, 95–99.

161 F.-Q. Liu, H. Wu, T. Li, L. R. Grabstanowicz, K. Amine and T. Xu, *Nanoscale*, 2013, **5**, 6422.

162 Y. F. Yuan, Y. B. Pei, J. Fang, H. L. Zhu, J. L. Yang and S. Y. Guo, *Mater. Lett.*, 2013, **91**, 279–282.

163 J. Gao, M. A. Lowe and H. D. Abruña, *Chem. Mater.*, 2011, **23**, 3223–3227.

164 W. Xu, J. Wang, F. Ding, X. Chen, E. Nasybulin, Y. Zhang and J.-G. Zhang, *Energy Environ. Sci.*, 2014, **7**, 513–537.

This journal is © The Royal Society of Chemistry 2022

J. Mater. Chem. A, 2022, **10**, 14221–14246 | **14245**

165 D. Lin, Y. Liu and Y. Cui, *Nat. Nanotechnol.*, 2017, **12**, 194–206.

166 J. Chen, J. Zhao, L. Lei, P. Li, J. Chen, Y. Zhang, Y. Wang, Y. Ma and D. Wang, *Nano Lett.*, 2020, **20**, 3403–3410.

167 J. Li, P. Zou, S. W. Chiang, W. Yao, Y. Wang, P. Liu, C. Liang, F. Kang and C. Yang, *Energy Storage Mater.*, 2020, **24**, 700–706.

168 W. Li, J. Liu and D. Zhao, *Nat. Rev. Mater.*, 2016, **1**, 16023.

169 Y. Ma, A. Huang, H. Zhou, S. Ji, S. Zhang, R. Li, H. Yao, X. Cao and P. Jin, *J. Mater. Chem. A*, 2017, **5**, 6522–6531.

170 Y. Zhu, M. Yang, Q. Huang, D. Wang, R. Yu, J. Wang, Z. Zheng and D. Wang, *Adv. Mater.*, 2020, **32**, 1906205.

171 S. Ponnada, M. S. Kiai, D. B. Gorle, S. Rajagopal, S. Andra, A. Nowduri and K. Muniasamy, *Energy Fuels*, 2021, **35**, 11089–11117.

172 B. Liu, Y. Zhang, Z. Wang, C. Ai, S. Liu, P. Liu, Y. Zhong, S. Lin, S. Deng, Q. Liu, G. Pan, X. Wang, X. Xia and J. Tu, *Adv. Mater.*, 2020, **32**, 2003657.

173 B. Duan, W. Wang, H. Zhao, A. Wang, M. Wang, K. Yuan, Z. Yu and Y. Yang, *ECS Electrochem. Lett.*, 2013, **2**, A47–A51.

174 X. Zhang, W. Wang, A. Wang, Y. Huang, K. Yuan, Z. Yu, J. Qiu and Y. Yang, *J. Mater. Chem. A*, 2014, **2**, 11660–11665.

175 K.-N. Jung, J. Kim, Y. Yamauchi, M.-S. Park, J.-W. Lee and J. H. Kim, *J. Mater. Chem. A*, 2016, **4**, 14050–14068.

176 H. Wang, J. Li, F. Li, J. Li and J. Xu, *Chem. Res. Chin. Univ.*, 2020, **36**, 1153–1160.

177 S.-W. Kim, D.-H. Seo, X. Ma, G. Ceder and K. Kang, *Adv. Energy Mater.*, 2012, **2**, 710–721.

178 C. Vaalma, D. Buchholz, M. Weil and S. Passerini, *Nat. Rev. Mater.*, 2018, **3**, 18013.

179 Q. Wang, J. Xu, W. Zhang, M. Mao, Z. Wei, L. Wang, C. Cui, Y. Zhu and J. Ma, *J. Mater. Chem. A*, 2018, **6**, 8815–8838.

180 H. Li, C. Wu, Y. Bai, F. Wu and M. Wang, *J. Power Sources*, 2016, **326**, 14–22.

181 J. F. Parker, I. R. Pala, C. N. Chervin, J. W. Long and D. R. Rolison, *J. Electrochem. Soc.*, 2016, **163**, A351–A355.

182 J. F. Parker, C. N. Chervin, I. R. Pala, M. Machler, M. F. Burz, J. W. Long and D. R. Rolison, *Science*, 2017, **356**, 415–418.

183 J. F. Parker, E. S. Nelson, M. D. Wattendorf, C. N. Chervin, J. W. Long and D. R. Rolison, *ACS Appl. Mater. Interfaces*, 2014, **6**, 19471–19476.

184 J. S. Ko, A. B. Geltmacher, B. J. Hopkins, D. R. Rolison, J. W. Long and J. F. Parker, *ACS Appl. Energy Mater.*, 2019, **2**, 212–216.

185 F. Ren, Y. Ji, S. Tan and F. Chen, *Inorg. Chem. Front.*, 2021, **8**, 72–78.

186 M. Jin, G. Zhang, F. Yu, W. Li, W. Lu and H. Huang, *Phys. Chem. Chem. Phys.*, 2013, **15**, 1601–1605.

187 S. Li, L.-L. Yu, R.-B. Li, J. Fan and J.-T. Zhao, *Energy Storage Mater.*, 2018, **11**, 176–183.

188 N. M. Shinde, Q. X. Xia, J. M. Yun, P. V. Shinde, S. M. Shaikh, R. K. Sahoo, S. Mathur, R. S. Mane and K. H. Kim, *Electrochim. Acta*, 2019, **296**, 308–316.

189 Y. S. Park, W.-S. Choi, M. J. Jang, J. H. Lee, S. Park, H. Jin, M. H. Seo, K.-H. Lee, Y. Yin, Y. Kim, J. Yang and S. M. Choi, *ACS Sustainable Chem. Eng.*, 2019, **7**, 10734–10741.

190 X. Zeng, Q. Jiao, N. Li and J. Wang, *Appl. Surf. Sci.*, 2020, **513**, 145785.

191 C. Deng, F. Ding, X. Li, Y. Guo, W. Ni, H. Yan, K. Sun and Y. M. Yan, *J. Mater. Chem. A*, 2015, **4**, 59–66.

192 N. A. Nguyen, V. T. Nguyen, S. Shin and H. S. Choi, *J. Alloys Compd.*, 2019, **789**, 163–173.

193 Y. Chen, C. Dong, J. Zhang, C. Zhang and Z. Zhang, *J. Mater. Chem. A*, 2018, **6**, 8430–8440.

194 W. Xu, S. Zhu, Y. Liang, Z. Cui, X. Yang and A. Inoue, *J. Mater. Chem. A*, 2018, **6**, 5574–5579.

195 K. Zhang, X. Xia, S. Deng, Y. Zhong, D. Xie, G. Pan, J. Wu, Q. Liu, X. Wang and J. Tu, *Nano-Micro Lett.*, 2019, **11**, 1–11.

196 S. V. Sheen Mers and V. Ganesh, *SN Appl. Sci.*, 2020, **2**, 1–14.

197 N. A. Nguyen, V. T. Nguyen, S. Shin and H. S. Choi, *J. Alloys Compd.*, 2019, **789**, 163–173.

198 H. Ren, Y. Deng, Y. Zhao, Z. Xing, X. Dong, H. Shi, Q. Yin and Z. Ju, *J. Mater. Sci.*, 2018, **53**, 13090–13099.